Chapter 6

Flexural Study of Beams: Numerical Investigation

6.1 Introduction

The flexural response of the beams with and without cutout as well as stiffening elements is determined using finite element software such as ABAQUS. Software ABAQUS is a commercial finite element analysis code, developed by Hibbitt, Karlsson & Sorensen, Inc and now it is maintained and serviced by SIMULIA Corporation. This software is a general-purpose tool which is the basic platform for numerical study of linear and nonlinear (material, geometrical and contact) problems. ABAQUS consists of three main parts such as ABAQUS/CAE, ABAQUS/Standard and ABAQUS/Explicit. ABAQUS/CAE is used to simulate the normal to complex problems and provides the graphical interface for pre- and post-processing needs. In other words, ABAQUS/CAE is a consistent interface for creating, submitting, monitoring, and evaluating results from ABAQUS/Standard and ABAQUS/Explicit simulations (ABAQUS, 2013). ABAQUS/CAE is divided into 10 modules such as Part, Property, Assembly, Step, Interaction, Load, Mesh, Job, Visualization, and Sketch. Each module is necessary for modelling and analyzing results. With the completion of each module, input file generates which has to be submitted to ABAQUS/Standard or ABAQUS/Explicit for analysis. ABAQUS/CAE has no inbuilt system of units and hence all input data are given in consistent units, i.e., SI, MKS units, etc. ABAQUS/Standard analysis tool is particularly well-suited to simulations which are static linear and nonlinear, linear dynamic, low-speed (low frequency response), nonlinear dynamic, nonlinear heat transfer, coupled temperature-displacement (quasi-static), coupled thermal-electrical, mass diffusion problems and structural-acoustics (ABAQUS, 2013).

ABAQUS/Explicit can analyze the problems which are high-speed (short duration) dynamics, drop tests and crash analyses of structural members, large, nonlinear, quasi-static analyses, deep drawing, blow molding, and assembly simulations, highly discontinuous post buckling and collapse simulations and coupled temperature-displacement (dynamic) problems.

This chapter presents the modelling techniques for simulating the three-point bending test of FRP I-beams with bearing plates, stiffeners and different stiffening elements such as cover angle, cover plate, and web plates. Moreover, numerical simulation of castellated beams is also presented in this chapter. The main objective of numerical modelling is to simulate the FRP I-beam, to predict the response and failure modes similar to that of experimental investigation. This model can be further utilized for investigation of FRP I-

beams with different geometric configurations, stiffening elements and cutouts. The detailed description of modelling technique and analysis procedure is explained next. The following section also highlights the measures to be taken while modeling the beams with stiffening elements.

6.2 Modelling of FRP beams

6.2.1 Part module

In this module, deformable shell planer parts are used to produce flanges and web of I-beam. Stiffening elements such as cover angle, cover plate, carbon fiber layers, bearing stiffener, splice plate and web plate are also made by 3D deformable shell, while the non-deformable discrete rigid part is used for simulation of bearing plates. It is because bearing plates provided in experimental tests were steel plates, and flexural rigidity of plate was much higher than that of FRP beam. A reference point is also provided on the part, which is rigidly self-connected with bearing plate as shown in Fig. 6.1(a). This reference point is used to provide boundary and loading conditions to bearing plate. In order to provide interaction between bearing plate and I-beam, shape is converted from solid to shell. Final, rigid bearing plate is a hollow from inside and the plate is non-deformable rigid part as illustrated in Fig. 6.1(b).

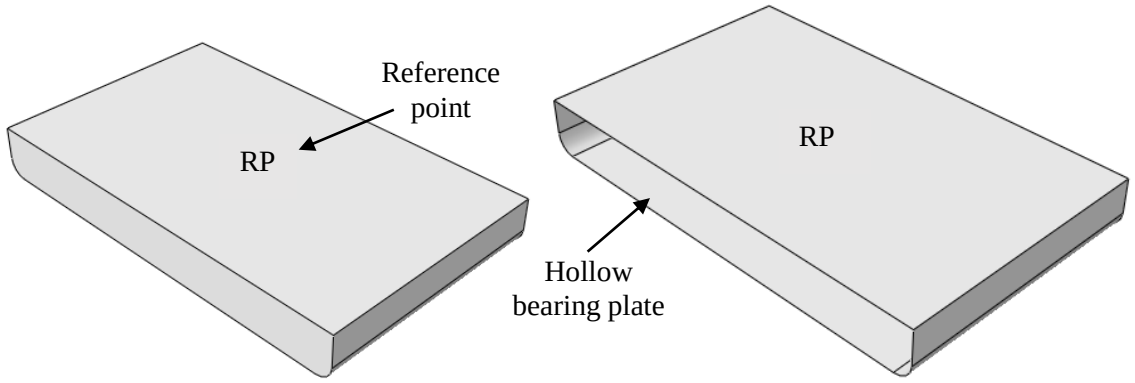

(a) Isometric view (b) Inside view (removing the selected surface)

Fig. 6.1. Discrete rigid shell bearing plate.

Castellated beams are also modelled using S4 shell element. Like in experimental investigation, firstly two T-sections (see Fig. 6.2) were made, later both are connected together. The connection of both T-sections is described in the following sections.

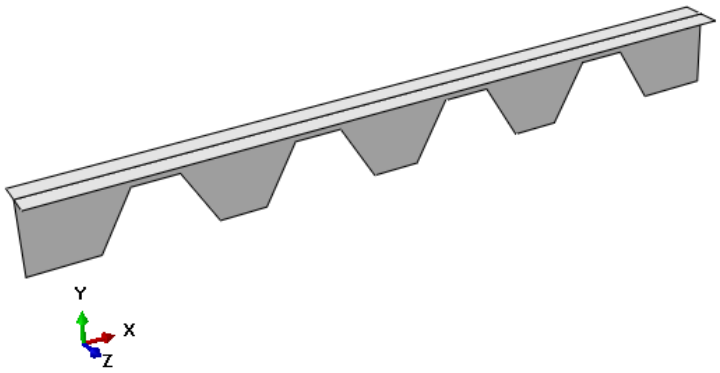

Fig. 6.2. Half part of castellated beam.

6.2.2 Material properties

FRP beams and stiffeners are assigned with orthotropic material properties, via using option "elastic lamina" in material gallery ABAQUS. In order to assign properties to the part, a section is created using composite layup manager. Thickness and orientation of plies and integration points are specified in that composite layup manager. Properties are assigned to each panel (surface) of the beams and stiffeners. In this analysis, Simpson integration rule is selected, and one integration point is taken at center of each element. This facilitates the measurement of stresses in each element.

6.2.3 Assembly module

In this module, all parts are assembled together, for example flanges and web panels, which are made separately, are connected together (flanges are perpendicular to the web) using merge tool to produce I-section. Similarly, stiffeners are also made by merging the separate panels as per the required cross-section. For example, to make T-shaped stiffener, web and flange of T-shape stiffeners are made as a rectangular panel.

6.2.4 Meshing properties

During analysis of FEM models, it is observed that size of mesh finer than 0.008 x 0.008 m does not affect the results significantly but increases the computational time. Hence, mesh size of I-beam, stiffening element and bearing plate is kept around 0.008 m. I-beam is modeled with four-noded linear shell elements with reduced integration, i.e., S4R (ABAQUS, 2013). Beam is meshed with quadrilateral elements of size 0.008 x 0.008 m. Bearing plates are non-deformable discrete rigid shell element, so they are assigned with a 4-node 3-D bilinear rigid quadrilateral (R3D4) element. In order to assign the master surface to bearing plate in surface interaction with beam (interaction between bearing plate and beam), the mesh size of

bearing plate (0.0085 x 0.0085 m) is little coarser than that of beam (0.008 x 0.008 m). It is because, for proper interaction mesh of master surface should be coarser than mesh of slave surface. The number of elements in bearing plate under loading and over supports is 379 and 88, respectively. Surface of stiffening elements is considered as master surface in interaction module. Thus, stiffening element are simulated with four-nodded linear shell elements (S4R) and with mesh size 0.00825 x 0.00825 mm, which is coarser than I-beam.

6.2.5 Loading

In ABAQUS, flexural behavior of the beams can be investigated in load control or deflection control method. These both options are available in load module. In load control method, maximum load is specified and the ABAQUS run the program till maximum load is reached. The rate of loading is based on number of increments specified in step module. With each increment of load, deflections, rotations, stresses, strains, etc, is determined. Moreover, in the deflection control method, a value of deflection and/or rotation is specified in a particular or various directions. Thus, with each increment of deflection, internal forces, stresses, strains and moments are calculated and the analysis terminate when the maximum deflection is reached. Load control method is simple and easy method because applied load can be measured directly, which is helpful in plotting the load-deflection curves, while in deflection control method, lot of calculations has to be done, which is time consuming. Hence, this flexural study of FRP beams is performed in load control. A transverse concentrated load is applied on a central reference node of bearing plate and this load is transferred to the beam as a uniformly distributed load on the contact surface area between the beam and bearing plate. Like mechanical properties, boundary conditions also play an important role to get the good agreement of numerical results with experimental results. Therefore, in order to simulate the boundary conditions of experimental test setup, vertical and longitudinal displacements of beam is controlled by assigning the boundary conditions on bearing plates over supports, and the lateral deflection and torsion of ends of the beam are restrained by assigning the boundary condition at the ends of the beam as shown in Fig. 6.3.

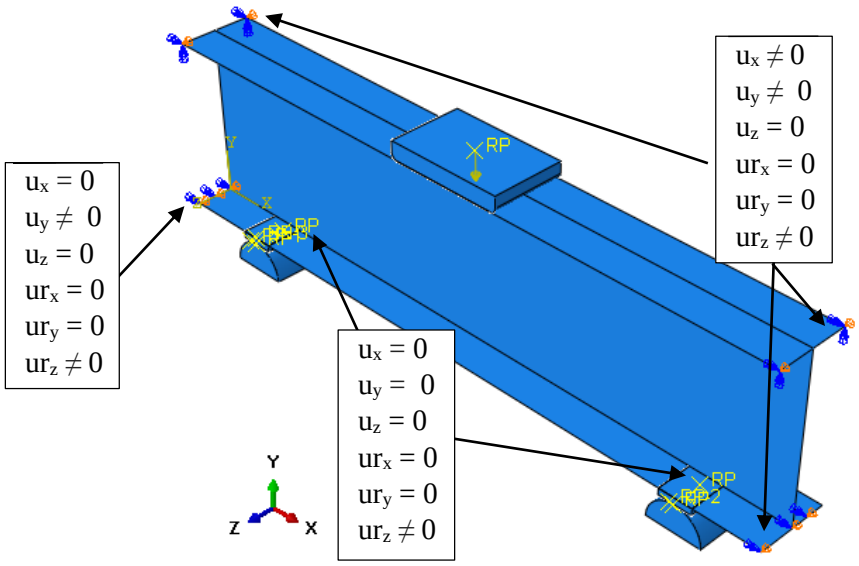

Fig. 6.3. ABAQUS model of I-beam having concentrated load on the center of bearing plate and have simply supported boundary conditions.

6.2.6 Interaction

In this simulation, 'surface-to-surface' interaction is assigned between beam and bearing plates. The contact property in tangential direction is given 'penalty' and the friction coefficient is taken as 0.3. In the normal direction, contact property is assigned as hard contact. All stiffening elements other than carbon fiber layers are connected with beams using fasteners and the top edge of the vertical stiffener is connected with flange by tie-connection. Alongwith bolted connection, 'surface-to-surface' interaction is also assigned to the interface between the stiffening elements and the beam. Analytical as well as numerical modeling is based on perfect bond between the stiffening element and beam. This assumption is justified and confirmed by experimental observation, where debonding was not noticed in stiffened beams during testing. Therefore, carbon fibers are also attached to the web-flange junction with surface-to-surface interaction. In castellated beams, the connection between two T-sections is made by tie connection, and the splice plate over connection is attached using fasteners and 'surface-to-surface' interaction is also assigned between the splice plate and web of I-beam.

6.2.7 Analysis procedure

In the step module, ABAQUS/Standard analyzer tool is used to determine the flexural response of the FRP under three-point bending. In the simulation, firstly linear buckling analysis is performed to determine the first buckling mode of the beam using Eigen value procedure. Further, using Riks method, post-buckling behavior of beam is predicted for first mode shape with imperfection of 0.1% of the depth of beam. During

analysis, it is noted that sizes of imperfection hardly effected the flexural response of the beams. After the analysis of each stiffened and unstiffened beam, post-processing of data is performed by evaluating the failure load using the delamination failure criterion, i.e., Eq. (5.56). In the castellated beams, failure load is predicted using Eq. (5.56) and Eq. (6.1). The minimum of both loads obtained from these two equations is considered as failure load of castellated beam.

$$\left(\frac{\sigma_{lb}}{S_{lb}}\right)^{2.5}+\left(\frac{\tau_{xz}}{S_{xz}}\right)^{2.5}\geq 1 \tag{6.1}$$

where σ_{lb}, and τ_{xz} are the longitudinal compressive bending stress and shear stress, respectively. Corresponding strengths such as bending compressive and shear strengths are represented by S_{lb}, and S_{xz}, respectively.

6.3 Comparison of experimental, analytical and numerical responses

This section presents the verification of flexural responses obtained from analytical and numerical modeling with respect to the experimental response. Beams PULT-B and PULT-C are modelled using the mechanical properties given in Table 3.9 (Chapter 3). Flexural response is verified for beams having (L/d) ratios of 7 with bearing plates and different stiffening elements. Further, the flexural response is determined for beams having bearing plates and stiffeners for length-to-depth ratios of 3 and 5. Delamination failure criterion Eq. (5.56) is used to determine the failure load of stiffened beams. The comparison of predicted analytical and numerical responses with experimental response is discussed as follow.

6.3.1 Beam with bearing plate

The critical buckling loads and crippling strength determined from different design formulae are presented in Table 6.1. It is observed that critical lateral-torsional buckling load of the beams determined from analytical equations is much higher than that of the experimental load, which confirms that failure is not due to the lateral-torsional buckling of beams. Moreover, critical local buckling load of the beam is also higher than the experimental buckling load, while the failure load predicted from failure criterion is equivalent to the experimental load. The same failure criterion is used in the FEM model to get the failure load and gives the load closer to that of experimental results. During bending of beam, rigid bearing plate applies the load over the flange in the form of two concentrated loads as shown in Fig. 6.4(a). From the FEM study, it is noted that if the failure criterion (Eq. 5.56) is not incorporated in the modeling, then the beam undergoes local buckling of compression flange and web (see Figs. 6.4(b) and (c)), which confirms the findings of the Borowicz and Bank (2014). Authors concluded that failure of the web-flange junction

of beams having L/d ratio 3 is due to the local buckling of web. However, in this study the failure load obtained from failure criterion is lower than the critical local buckling load of the beam (flange and web) and is closer to the experimental buckling load. Fig. 6.5 shows that the slope of numerical and analytical responses is nearly same and both models provide the close approximation with experimental response, but the failure strength of the beams predicted from numerical model is more closer to the experimental than the analytical strength. The experimental load-deflection responses of both beams (PULT-B and PULT-C) show that responses are linear until the complete failure of the specimen, i.e., no ply failed before the complete failure or rupture of the specimen. Specimens failed due to the crushing of web under web-flange junction. Hence, the failure load determined from failure criterion, i.e., Eq. (5.56) gives the good comparison of results with experimental values as presented in Table 6.1.

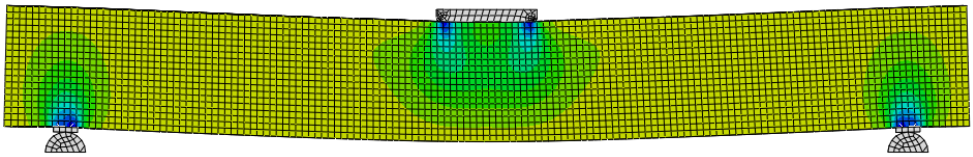

(a) Stress contour under the loading

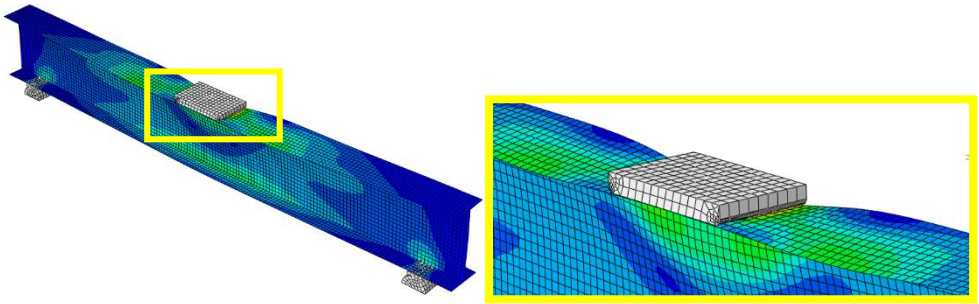

(b) Local buckling of the Flange

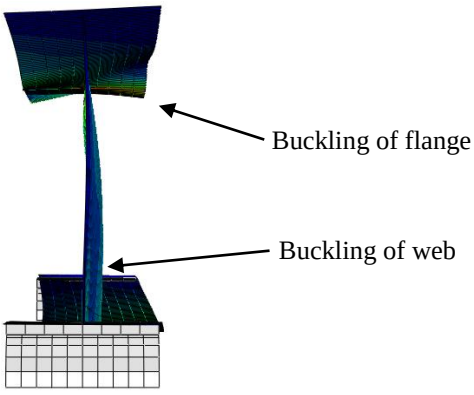

(c) Local buckling of web.

Fig. 6.4. Failure mode of the beam with bearing plate.

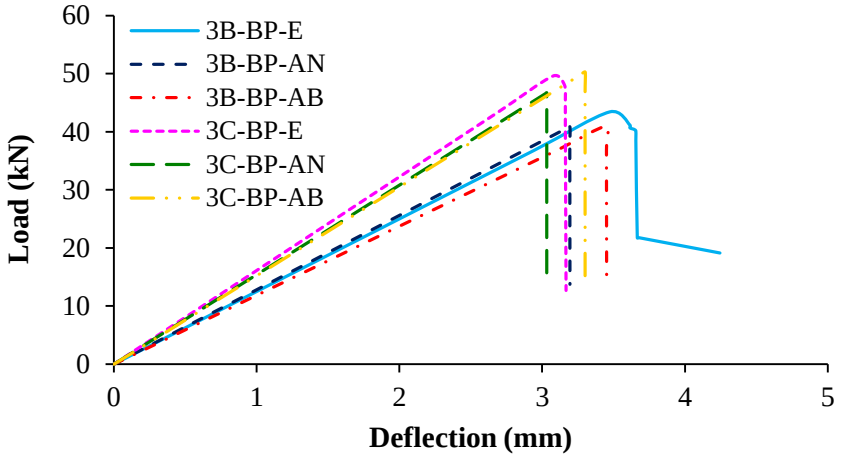

(a) L/d = 3

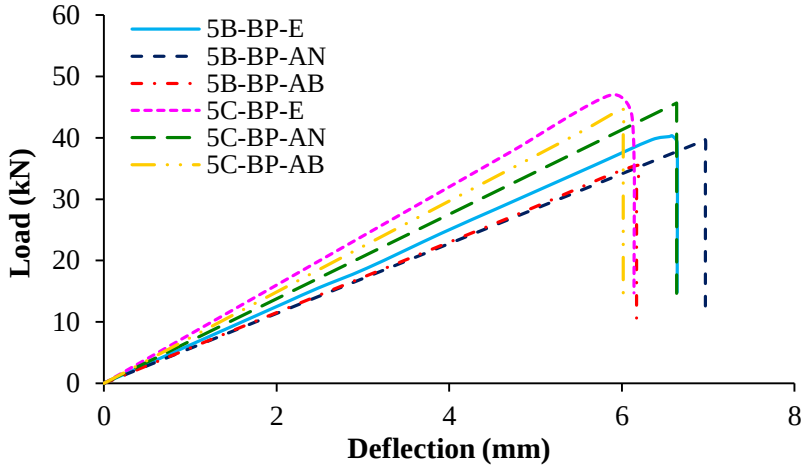

(b) L/d = 5

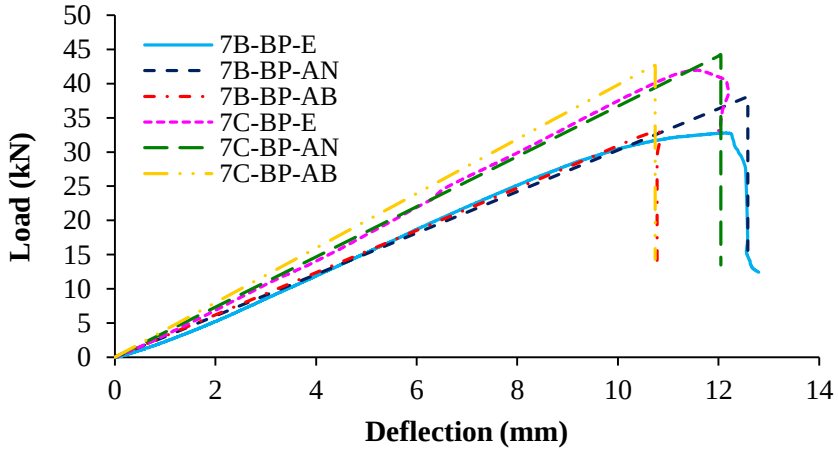

(c) L/d = 7

Fig. 6.5. Comparison of flexural responses of beams having different L/d ratios. ('E' is experimental, 'AN' is analytical and 'AB' is ABAQUS response)

6.3.2 Beam with bearing plate and bearing stiffeners

The comparison of failure load of the beams obtained from analytical, numerical and experimental investigation is presented in Table 6.2. The lateral-torsional buckling load of the beam determined from analytical equation is higher than the experimental failure load. It is also observed that critical local buckling load of flange obtained from Eq. (5.35) is approximately equal to the experimental failure load of the beam PULT-C having L/d ratio 7 (7C-TS-AS), while for other L/d ratios the failure load obtained from the equations is significantly higher or lower. Even though, the failure load obtained from Eq. (5.35) is approximately equal to the experimental load but still this equation cannot be used because the local buckling of compression flange was not observed in the beam during testing. In contrast, the failure load of beams obtained from failure criterion (Eq. 5.56) gives the good agreement of results with experimental results. It is noted that with addition of T-shaped stiffener, transverse stresses produced from bearing plate are reduced on the junction of web-flange of I-beam, which leads to the higher load carrying capacity of the beams. However, the diagonal bearing stress are still present in the beam, as a result failure criterion is satisfied at web under the bearing plate. The comparison of experimentally obtained load-vs-deflection curves with that of numerical and analytical models are depicted in Fig. 6.6. It is noted that flexural response obtained from numerical and analytical models are in close agreement with experimental response. Fig. 6.7 shows that distribution of stresses is same in all beams having different L/d ratios. The red region in beam shows the maximum stress and blue portion shows the minimum stress. The maximum stresses are observed under the bearing plate, which is due to compression produced from the loading, but the bearing plate provides strength to the flange. Hence, the flange does not fail under the bearing plate, while the web fails due to diagonal bearing stress. Therefore, stresses for failure criterion are satisfied at the vertical distance of "t_f+R" from bottom of flange and at slope of 1:2.5 from the edge of bearing plate as shown in Fig. 6.7. At this location, the load obtained from failure criterion is equivalent to the experimental failure load. Thus, it confirms that the failure mode of the beams obtained by tests is due to diagonal bearing stresses. It is also stated that ABAQUS model is effective in reproducing the same deformation as seen in experimental investigation.

Table 6.1 Comparison of experimental failure load (kN) with analytical and numerical failure loads (kN) of beams with bearing plate.

Specimen ID	Experimental	Analytical											Numerical	
		Lateral-torsional buckling of beam				Local buckling of web					Failure criterion, Eq. (5.56)	Ratio*	Failure Criterion Eq. (5.56)	Ratio*
		Euro code	Italian code	Pultex	ASCE Std.	Euro code	Italian code	ASCE Std.	Allen & Bulson (1980)	Borowicz & Bank (2011)				
3B-BP	43.42	1409.08	598.32	541.74	1256.55	43.98	348.23	341.40	88.95	123.14	40.86	0.94	40.92	0.94
5B-BP	40.31	288.38	239.29	111.66	260.16	43.98	208.94	204.84	80.05	123.14	39.67	0.98	35.46	0.87
7B-BP	32.78	103.71	126.13	40.57	95.11	43.98	149.24	146.31	77.60	123.14	38.07	1.16	32.94	1.00
3C-BP	49.63	1712.95	720.50	657.60	1373.33	64.62	510.31	484.90	89.72	179.89	46.72	0.94	50.30	1.01
5C-BP	46.98	350.30	288.54	135.35	284.39	64.62	306.19	290.94	80.69	179.88	45.65	0.97	44.64	0.95
7C-BP	41.93	125.84	152.21	49.08	103.99	64.62	218.70	207.81	78.20	179.89	44.18	1.05	42.65	1.01

*Ratio is w.r.t. experimental load

Table 6.2 Comparison of experimental failure load (kN) with analytical and numerical failure loads (kN) of beams with bearing plate and stiffeners.

Specimen ID	Experimental	Analytical										Numerical	
		Lateral-torsional buckling of beam				Local buckling of compression flange				Failure criterion, Eq. (5.56)	Ratio*	Failure criterion, Eq. (5.56)	Ratio*
		Euro code	Italian code	Pultex	ASCE Std.	Euro code	Italian code	Pultex	ASCE code				
3B-TS-AS	72.33	1409.08	598.32	541.74	1256.55	57.72	130.37	25.06	100.37	72.26	1.00	73.60	1.02
5B-TS-AS	72.13	288.38	239.29	111.66	260.16	33.54	78.22	15.044	60.22	65.94	0.91	69.45	0.96
7B-TS-AS	64.87	103.71	126.13	40.57	95.11	23.74	55.87	10.74	43.06	63.00	0.97	62.12	0.96
3C-TS-AS	91.94	1712.95	720.50	657.60	1373.33	63.31	186.48	39.54	129.10	90.88	0.99	96.71	1.05
5C-TS-AS	82.81	350.30	288.54	135.35	284.39	36.86	111.89	23.72	77.47	83.67	0.91	69.45	0.84
7C-TS-AS	83.75	125.84	152.21	49.08	103.99	26.10	79.92	16.94	55.33	76.60	0.91	80.61	0.96

*Ratio is w.r.t. experimental load

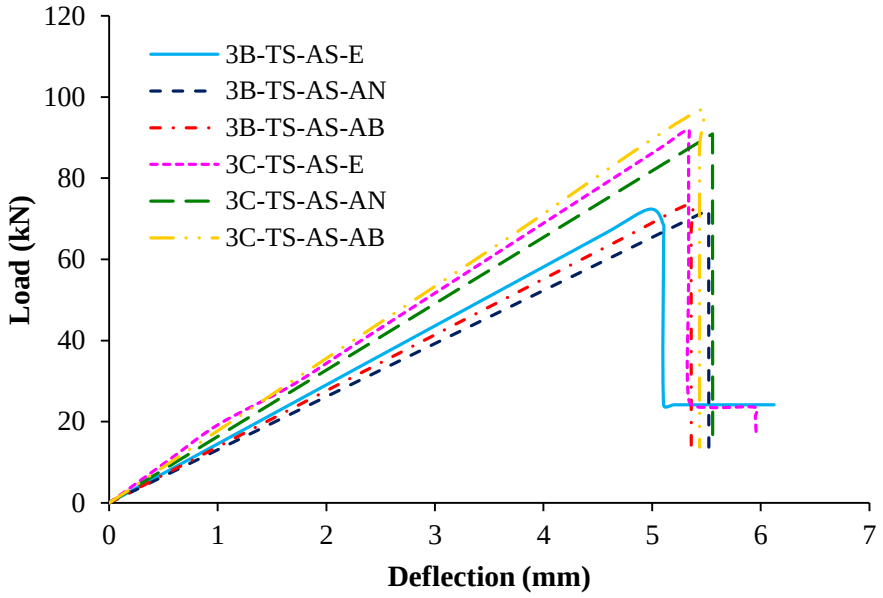
120
100
80
60
40
20
0
Load (kN)
0
1
2
3
4
5
6
7
Deflection (mm)
3B-TS-AS-E
3B-TS-AS-AN
3B-TS-AS-AB
3C-TS-AS-E
3C-TS-AS-AN
3C-TS-AS-AB

(a) L/d = 3

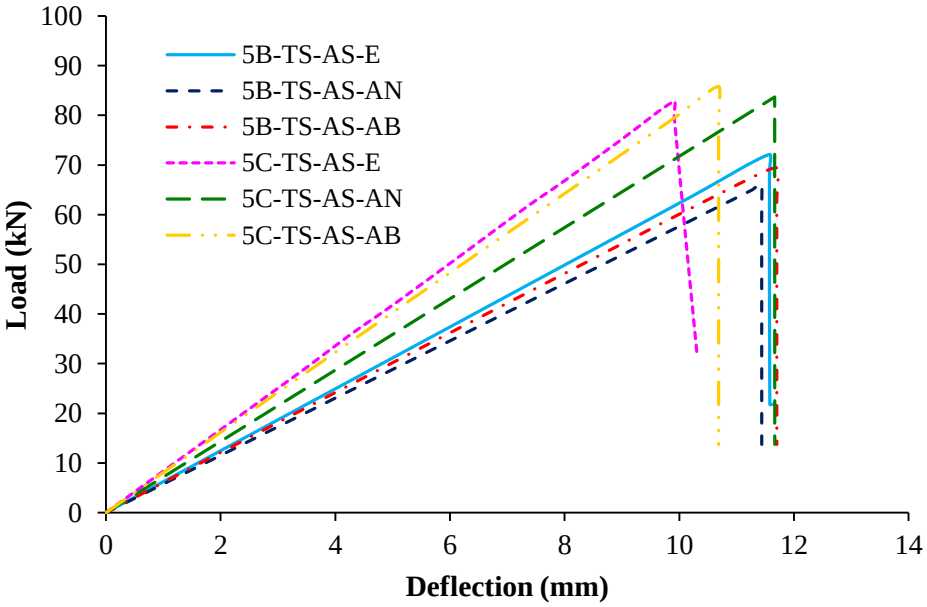
100
90
80
70
60
50
40
30
20
10
0
Load (kN)
0
2
4
6
8
10
12
14
Deflection (mm)
5B-TS-AS-E
5B-TS-AS-AN
5B-TS-AS-AB
5C-TS-AS-E
5C-TS-AS-AN
5C-TS-AS-AB

(b) L/d = 5

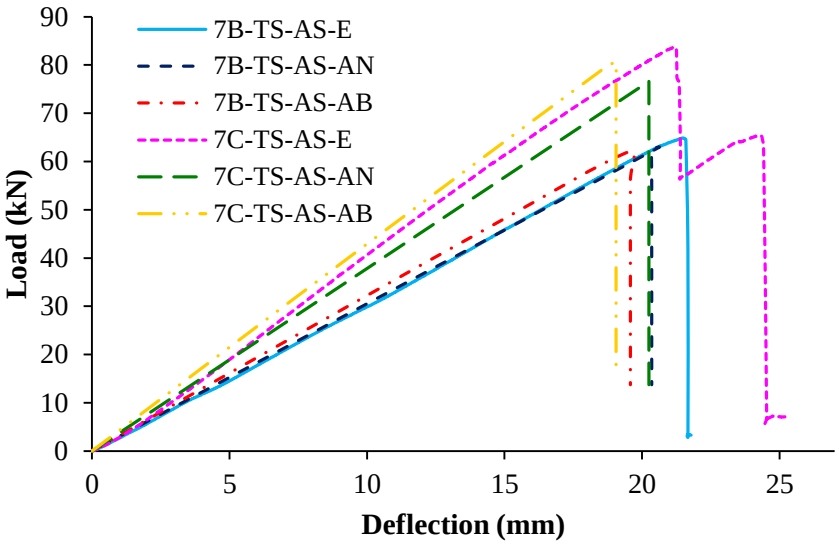

(c) L/d = 7

Fig. 6.6. Load-deflection responses of beams with bearing plate and bearing stiffeners.

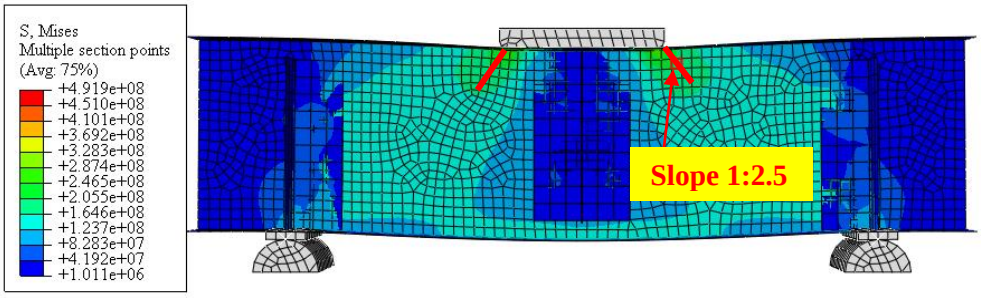

(a) L/d = 3

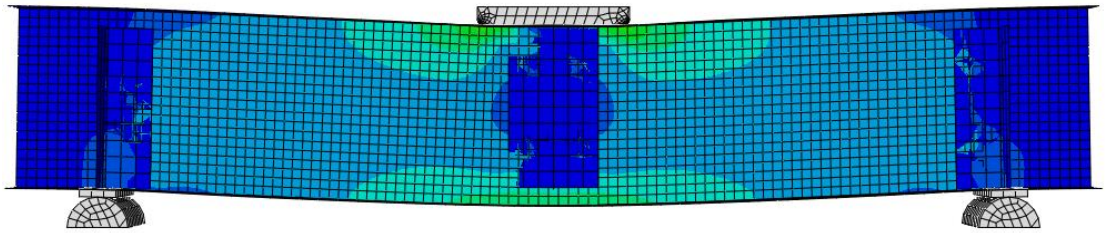

(b) L/d = 5

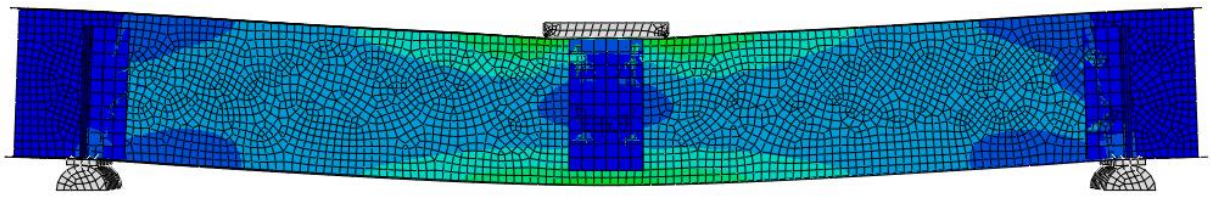

(c) L/d = 7

Fig. 6.7. Stress profile in beams of different length-to-depth (L/d) ratios.

6.3.3 Beam with bearing plate and stiffening elements

6.3.3.1 Cover angle

From the experimental investigation, it is observed that the beam with cover angle failed due to the delamination of fiber layers of compression flange. This failure is due to stress concentration produced from the change in geometry of the cross-section of the beam, i.e., at the end of the cover angle. From ABAQUS model, it is noted that the stress concentration is produced on the compression flange at the end of cover angle. This stress concentration is because of sudden change in the geometry of the beam (length of cover angle is lesser than that of beam) as well as flexural rigidity of angle section and beam is also different. Therefore, during bending of beam, stresses are higher at the end of cover angle as shown in Fig. 6.8(a). Hence, failure criterion is satisfied at this location and it gives the failure load closer to the experimental load. In order to consider the effect of stress concentration in the analytical model, a stress concentration factor (0.7) is multiplied with failure criterion. It is observed that with incorporation of stress concentration factor in analytical modeling, a good agreement with experimental results is achieved. The failure load obtained from analytical and numerical model is presented in Table 6.3. The load-vs-deflection response of the beam with cover angle is determined from Eq. (5.28) and is compared with numerical and experimental responses in Fig. 6.8(b). It is observed that slope of analytical and numerical models is almost same and little higher than experimental one.

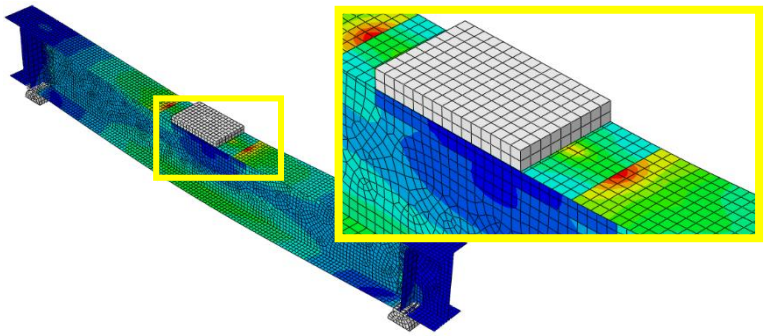

(a) Deformed shape

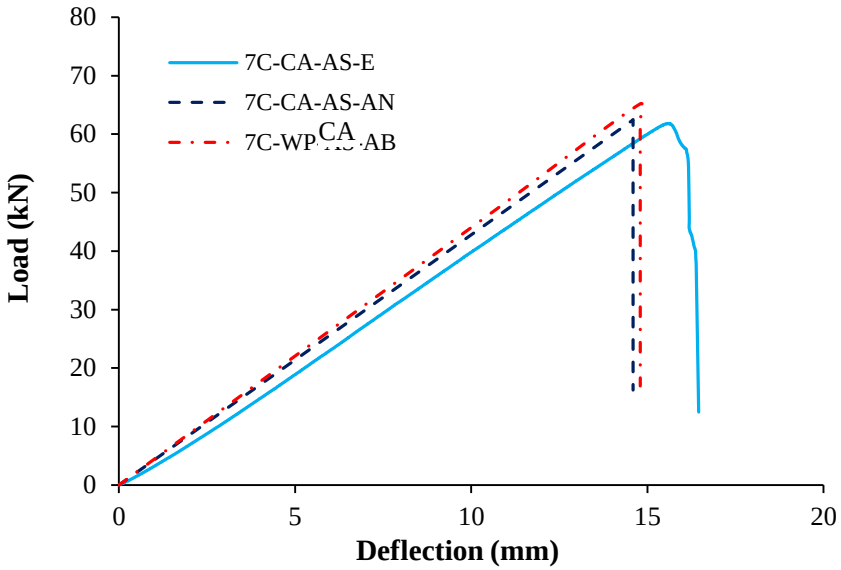

(b) Load-vs-deflection responses

Fig. 6.8. Beam stiffened with cover angle at compression web-flange junction.

Table 6.3 Comparison of experimental failure load (kN) with numerical and analytical failure loads (kN).

Specimen ID	Experimental	Analytical Eq. (5.56)	Analytical/ Experimental	Numerical	Numerical/ Experimental
7C-CA-AS	61.82	62.48	1.02	62.51	1.02
7C-CL-AS	66.12	66.23	1.01	67.90	1.03
7C-WP-AS	66.39	64.71	0.98	64.50	0.98
7C-CP	47.68	47.40	0.99	51.57	1.09

6.3.3.2 Carbon fiber layer

The deformed shape of the stiffened beam with carbon fiber layers is demonstrated in Fig. 6.9(a). Focusing on the stress concentration in beam, it is stated that delamination of layers of fibers seen in experimental study is due to the stress concentration produced under the bearing plate. Therefore, failure criterion (Eq. 5.56) also satisfies at this location and gives the failure load equal to the experimental load. Moreover, considering the stress concentration in analytical model produces the failure load of 66.23 kN, which is also equal to the load obtained from test, i.e., 66.12 kN. Fig. 6.9(b) depict both models yield the flexural response in close approximation to the experimental load. Hence, it is stated that FEM model is effective in showing the stress concentration and reproducing the same failure mode as seen in tests.

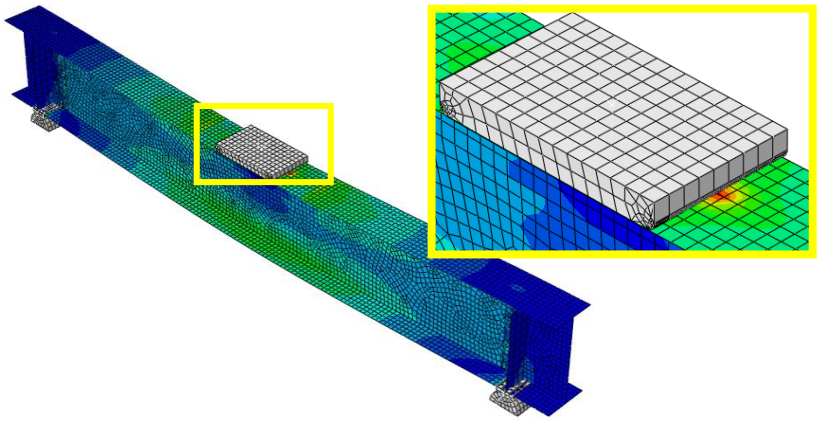

(a) Deformed shape

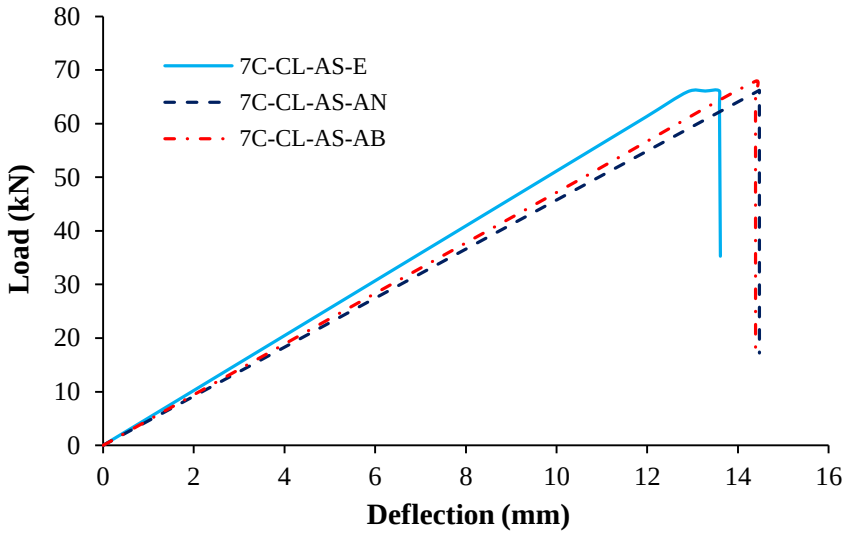

(b) Load-vs-deflection responses

Fig. 6.9. Beam stiffened with carbon fiber layers at compression web-flange junction.

6.3.3.3 Web plate

FRP I-beam is stiffened with web plate of size 160 x 110 mm (width x depth) at the mid span and connected by bolts (8 mm diameter). From the FEM model, it is observed that diagonal stresses produced by load bearing plate lead to the high stresses in the web at an angle 45^{o} as shown in Fig. 6.10(a). Thus, the failure criterion at this location give the failure load 64.50 kN that is equivalent to the experimental failure load 66.39 kN. The failure load obtained from the analytical model is 64.71 kN, which is 2.5% lesser than experimental load. Fig. 6.10(b) shows that both models yield the failure load in close approximation to the experimental failure load. It is also stated that the response obtained from numerical model as well as analytical model are little higher than the experimental response.

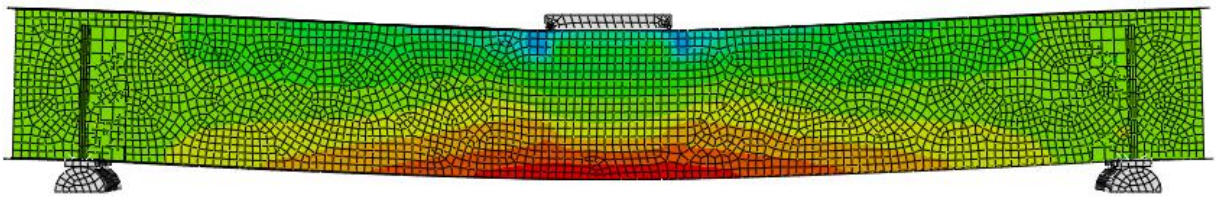

(a) Deformed shape

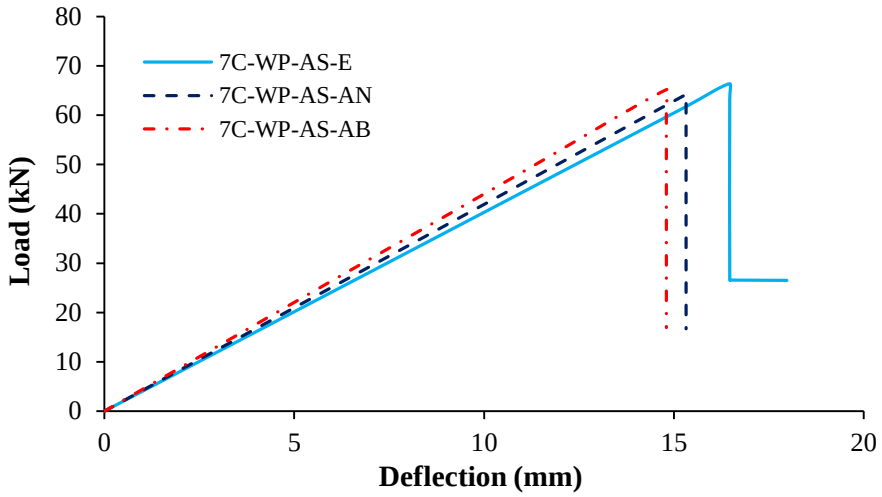

(b) Load-vs-deflection responses

Fig. 6.10. Beam stiffened with web plate at mid-span.

6.3.3.4 Cover plate

The stresses produced in FRP I-beam with cover plate under flexural loading is shown in Fig. 6.11(a). It is observed that due to absence of stiffening element under the web-flange junction, compressive stresses are high at the junction, which leads to the failure of the beam. Although stiffness of the beam with cover plate is higher than beam with bearing plate only, but the strength is nearly same. The failure criterion based on the Eq. (5.56) is used to determine the strength of the beam and Eq. (5.28) is used to evaluate the load versus deflection response of the beam. The comparison of numerical and analytical responses with experimental response is shown in Fig. 6.11(b). It is noted that both numerical and analytical models exhibit the same stiffness of the beam, while the slope of experimental response is little higher than both models.

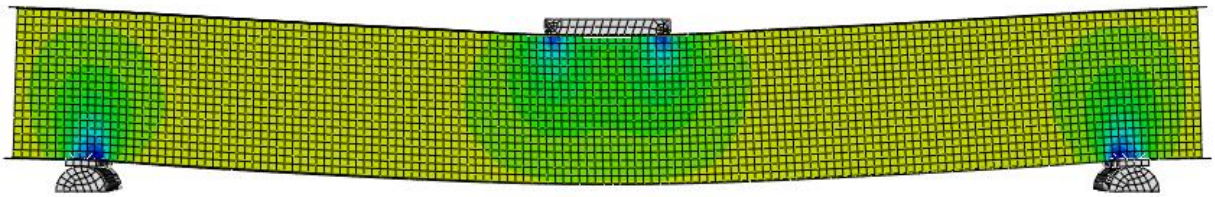

(a) Deformed shape

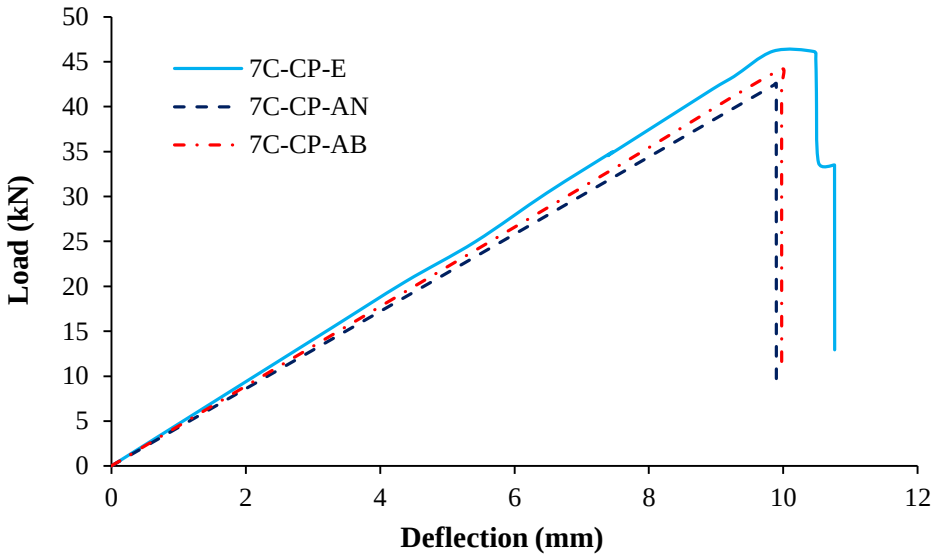

(b) Load-vs-deflection response

Fig. 6.11. Beam stiffened with cover plate at mid-span.

6.4 Parametric study on different sizes of beams and stiffeners

In the light of effective design of beams with and without stiffening elements, a parametric study is carried out on different material properties, length of bearing plates and stiffening elements on FRP I-beams. The mechanical properties of beam PULT-C and stiffening elements given in Table 3.9 (Chapter 3) are used for parametric study. In this study, standard dimensions of beams are taken as 150 x 65 x 1050 mm (depth x flange width x length) and the thickness (t) of web and flanges is 6.5 mm. Specially this section and the length of beam are chosen, because the beam with this section and length is less prone to buckling. Failure and service loads are determined for beams having width of flange-to-thickness ratio (b/t) varied from 5 to 15, depth-to-thickness ratio (h_w/t) varied from 21 to 40 and length-to-depth ratio (L/d) varied from 7 to 11. The beams having different b/t ratios have constant thickness of flanges and web (6.5 mm), depth (150 mm) and span length (1050 mm) of beam. In case of beams having different h_w/t ratios have flange width 65 mm, flange and web thickness 6.5 mm and length of 1050 mm, while beams having different L/d ratios have depth of beam 150 mm, flange width of 65 mm, with thicknesses of flanges and web equal to 6.5 mm each. Failure load is evaluated based on strength or buckling load of beams, while the service load is determined based on the load corresponding to the limit state of deflection of beam (L/300). The evaluation of failure load is also used to highlight the contribution of stiffening element in enhancing the strength of the beam, and the corresponding failure mode is helpful to decide the weaker portion of the beam. From the previous section, it is concluded that using failure criterion in analytical and FEM model gives good agreement of results with that of experimental test results, but the stress concentration or stress variation

seen in FEM model is missing in analytical modelling. Hence, FEM model is most suitable to be used for further parametric study on FRP beams. This parametric study is helpful in developing the guidelines for designing structures and is discussed in detail in the following sections:

6.4.1 Influence of length of bearing plate

Length of bearing plate is the most important parameter that affects the crushing load of the web. Hence, the effect of length of bearing plate on the flexural strength of beams is determined for different b/t, h_w/t and L/d ratios of beams. The comparison of variation in flexural strength of the beam having different b/t ratios with different sizes of bearing plate is shown in Fig. 6.12(a). In the legend of the figures, 'F' refers to failure load and 'S' refers to the service load. It is noted that failure load of the beams increases significantly with increase in a/L from 0.05 to 0.10, but with further increase in length of bearing plate (a/L), failure load of beams is almost constant, and the failure criterion is satisfied under the edge of bearing plate. It shows that crushing strength of the beams increases with increase in the length of bearing plate and becomes constant at a certain length of bearing plate. However, the service load is almost constant with increase in a/L ratio. In case of beam having different h_w/t ratios, it is noted that beam having h_w/t ratio 40 and with bearing plate of length 210 mm (a/L=0.15) has highest failure load (Fig. 6.12(b)). Moreover, for beams having h_w/t ratios varying from 21 and 30, failure load of the beams increases up to a/L equal to 0.15, and with further increased in a/L ratio, failure load decreases. Similarly, for beams having different L/d ratios, failure load is maximum at a/L equal to 0.15 (see Figs. 6.12(a) and 6.12(c)) and the same trend of failure load is seen in beams having different b/t ratios. From the study of variation in b/t, h_w/t and L/d ratios of beams, it is noted that ultimate load carrying capacity of the beams is same for a/L ratio more than 0.15 except for beam L/d = 3. It is because for a/L greater than 0.15, bearing plate produces the two-point loads on the web-flange junction which exhibits lower or same failure load of the beams having $a/L \leq 0.15$. Hence, in further parametric study, length of the bearing plate (a) is taken as 0.15L.

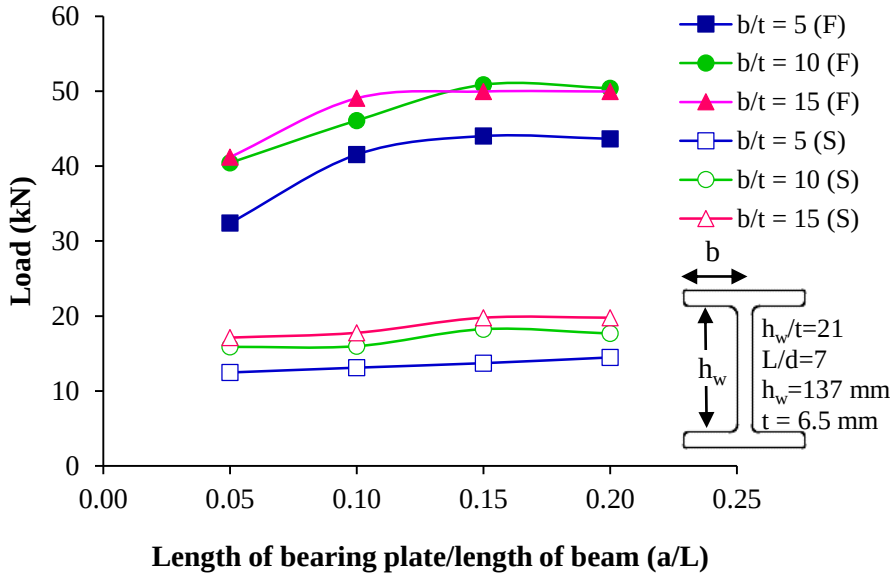

(a) Different width-to-thickness ratios (b/t) of beams

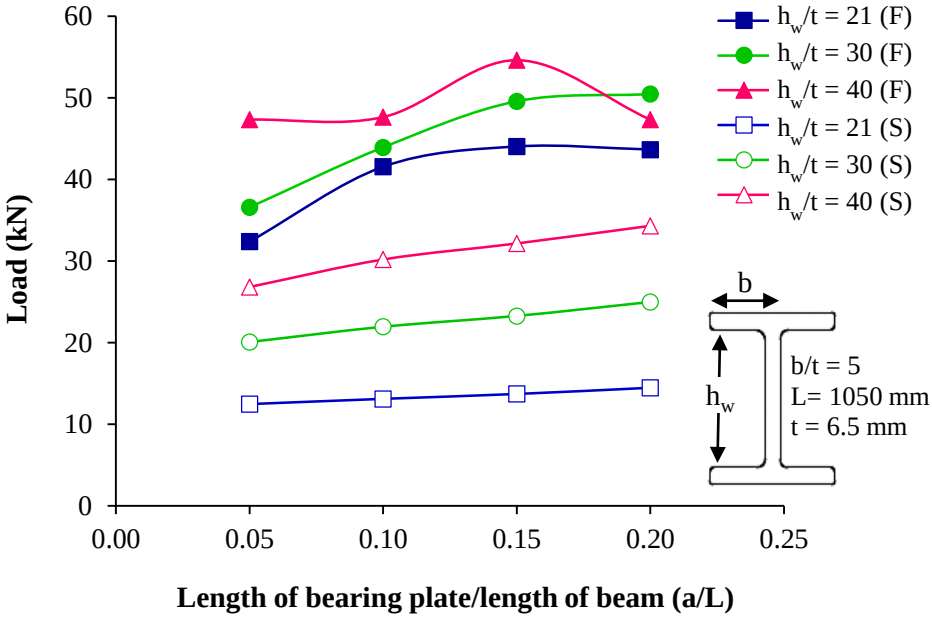

(b) Different depth-to-thickness ratios (h_w/t) of beams

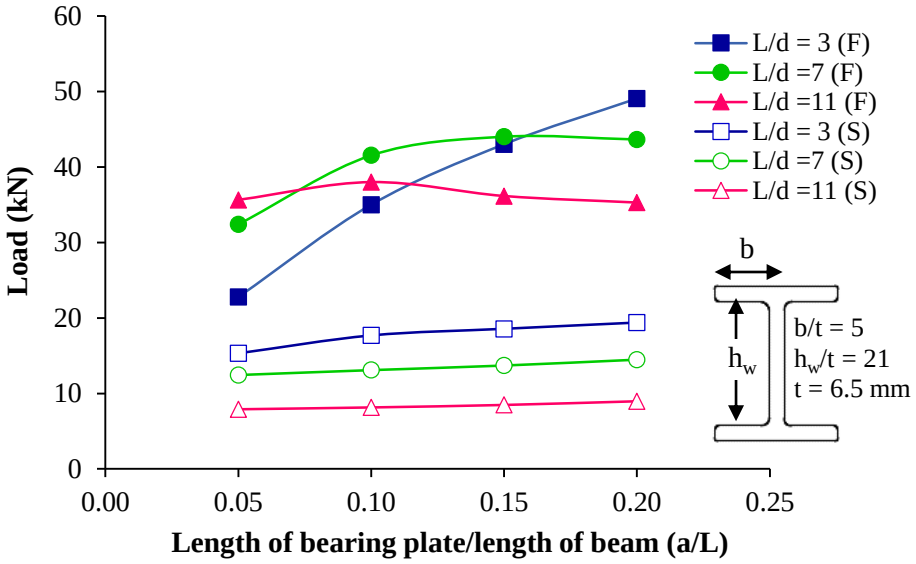

(c) Different length-to-depth ratios (L/d) of beams.

Fig. 6.12. Effect of length of bearing plate on the service and failure loads of beams.

6.4.2 Influence of transverse and shear modulus

Transverse and shear stiffnesses of FRP beams are very low in comparison with longitudinal stiffness. Therefore, it is important to study the effect of different transverse and shear moduli of beam on the service and failure loads of beams. Material properties of PULT-C given in Table 3.9 (Chapter 3) are used to study the effect of transverse modulus, keeping the longitudinal and shear modulus constant, while longitudinal-to-transverse Young's modulus ratio (E_1/E_2) is varied from 1 to 4. The failure and service loads of beams having different b/t and E_1/E_2 ratios are given in Fig. 6.13(a). It is noted that an increase in the E_1/E_2 ratio of the beams enhances the failure load of the beam with reduction in the service load of beams. It is because service load is directly proportional to the overall stiffness of the beams, which decreases due to the decrease in the E_2 with constant value of E_1 therefore service load decreases with decrease in stiffness of beams. Moreover, for a given loading, stresses produced in the beams also reduces because stress is directly proportional to the stiffness of the beams. Hence the failure load increases with decrease in the transverse modulus. In case of beams with different h_w/t ratios, failure load of beams increases with increase in the E_1/E_2 ratio of beams having h_w/t ratios 21 and 30, while the failure load of the beam with h_w/t ratio 40 decreases (see Fig. 6.13(b)) due to the buckling of web panel as shown in Fig. 6.14. The buckling is due to low transverse modulus and high h_w/t ratio. The same trend of results is seen in the study of L/d ratio (see Fig. 6.13(c)). Buckling is predominant for beam having L/d ratio 3, therefore failure load of the beams having E_1/E_2 ratios 3 and 4 is less than that for the beam having L/d ratio 7 for E_1/E_2 ratios 3 and 4.

Moreover, for other L/d ratios (7 and 11), failure load increases with an increase in the E_1/E_2 ratio of the beam.

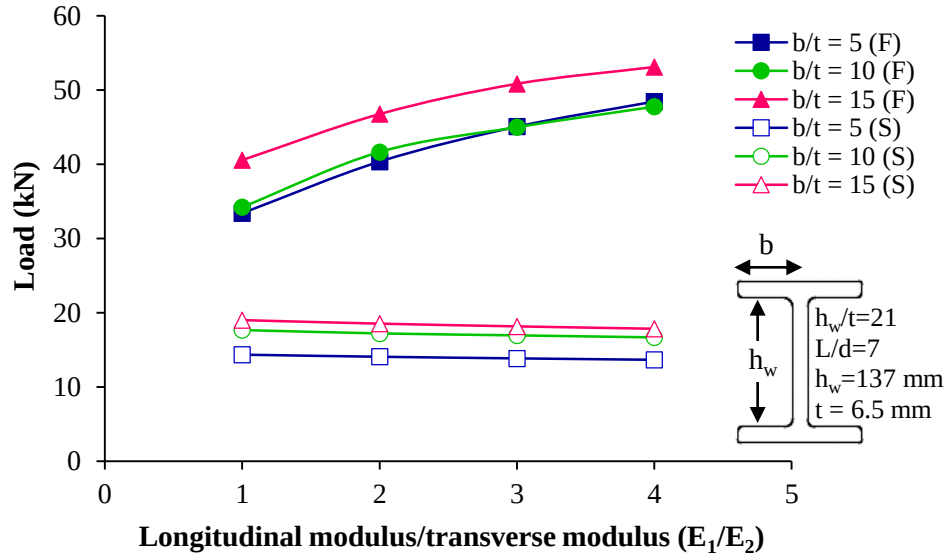

(a) Different width-to-thickness ratios (b/t) of beams

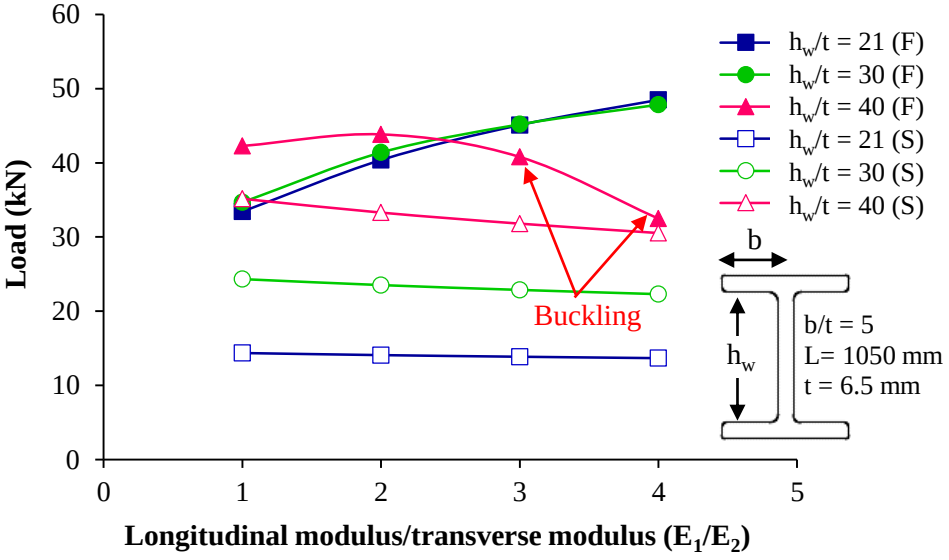

(b) Different depth-to-thickness ratios (h_w/t) of beams

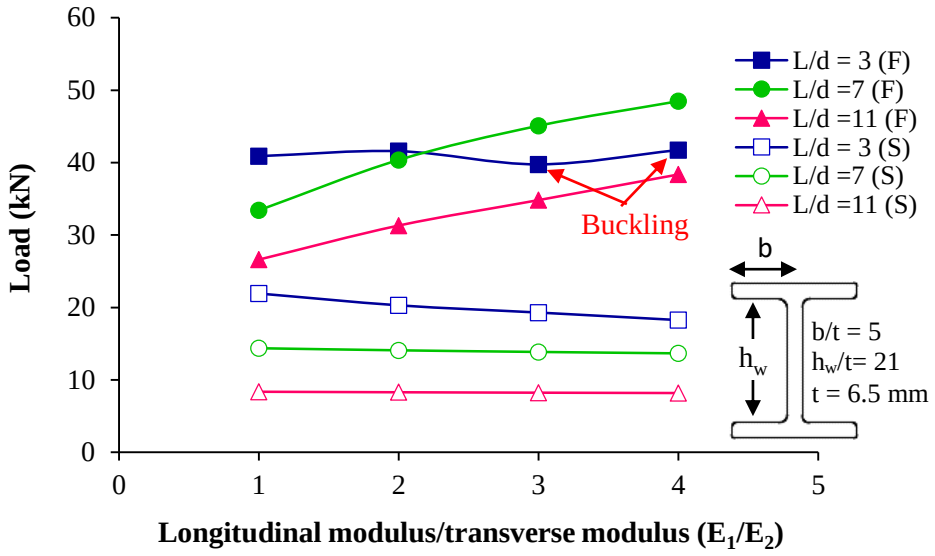

(c) Different length-to-depth ratios (L/d) of beams

Fig. 6.13. Effect of variation in transverse modulus on failure and service loads of beams.

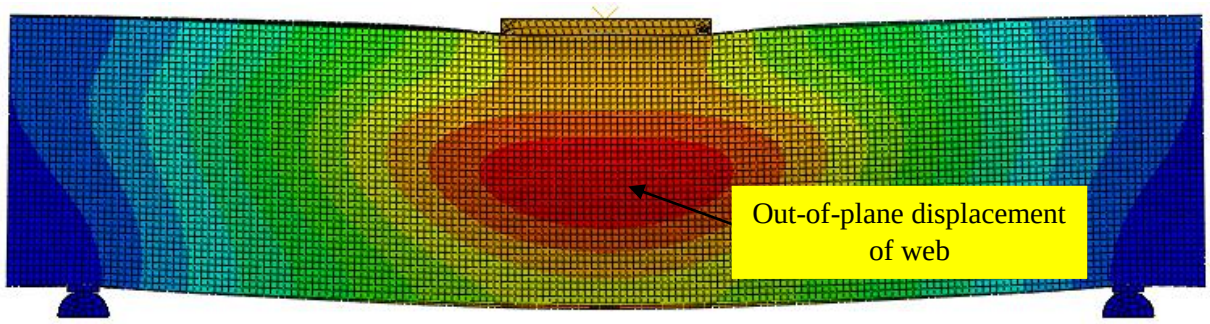

Fig. 6.14. Buckling of beam having h_w/t ratio 40, b/t ratio 5 and L/d ratio 7, with size of bearing plate 210 mm (a/L = 0.2).

In contrast to transverse modulus, failure load decreases with increase in longitudinal Young's modulus/shear modulus ratio (E_1/G_{12}) as shown in Figs. 6.15(a), (b) and (c). It is due to increase in the transverse stresses with decrease in shear stiffness of beams. Although flange width of beams having b/t ratio 15 is more than that of beams having b/t ratio 10, but its failure load is less. It is because of the buckling of flanges and web. Whilst the service load for b/t ratio 15 is higher than that of beams having b/t ratio 10 for lower value of E_1/G_{12}. The same trend of results is observed in beams having h_w/t ratios 40 and 30 as depicted in Fig. 6.15(b). As expected, service load of beams having h_w/t ratio 40 is higher than that of beams having h_w/t ratio 30, but the failure load is less than that of beams having h_w/t ratio 30, which is due to local buckling of web. In case of variation of L/d ratio, failure load seems to be almost same for all L/d ratio for given E_1/G_{12} ratio.

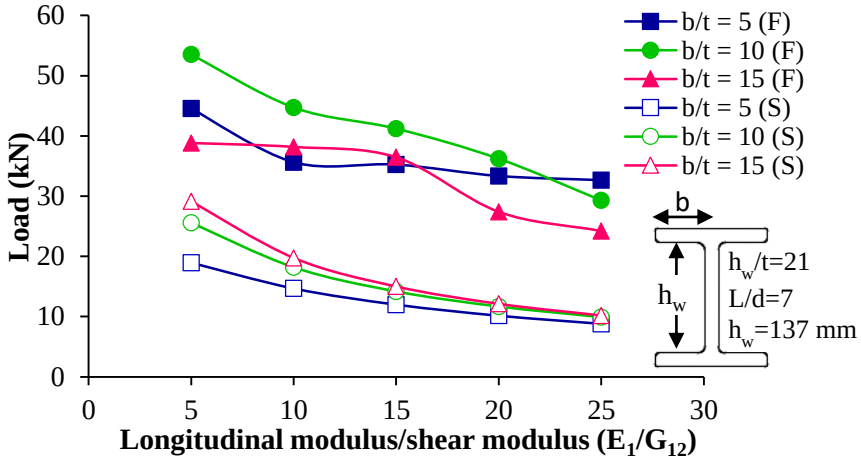

(a) width-to-thickness ratios (b/t)

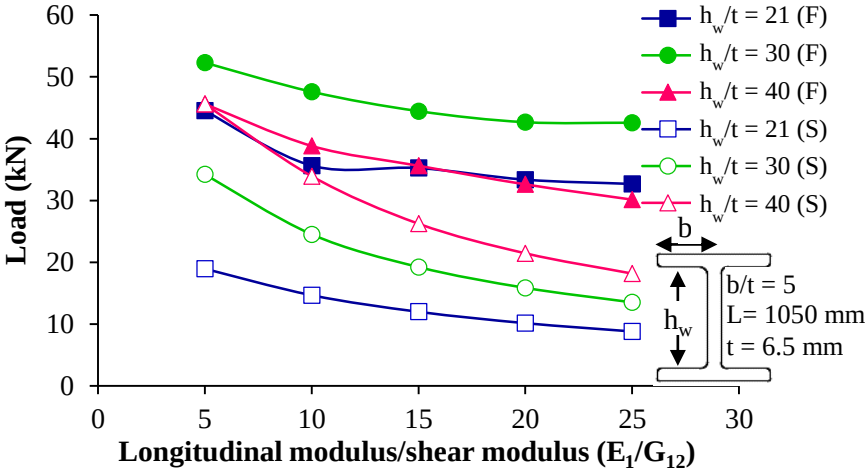

(b) depth-to-thickness ratios (h_w/t)

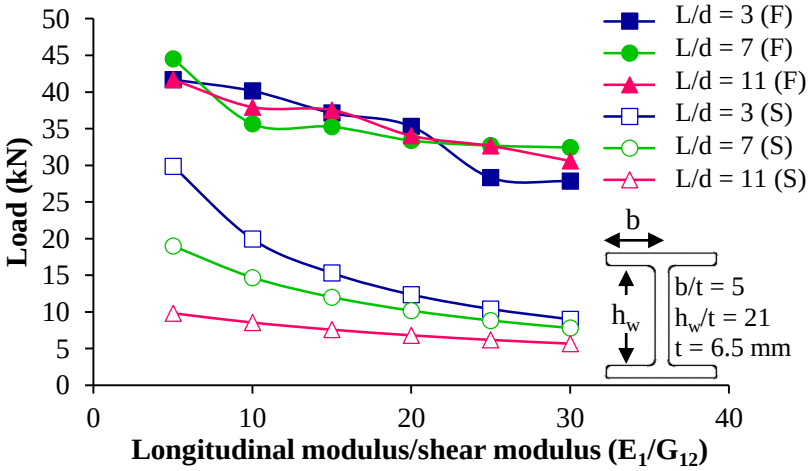

(c) length-to-depth ratios (L/d)

Fig. 6.15. Effect of variation in shear modulus on failure and service loads of beams.

6.4.3 Influence of length of bearing plate on T-shaped bearing stiffener

In this section, effect of different lengths of bearing plate on the strength of web-flange junction of I-beam and T-shaped bearing stiffener is studied. Failure and service loads are determined for bearing plate of lengths $0.7b_{tf}$, $1.4b_{tf}$, $2.1b_{tf}$, and $2.8b_{tf}$, where b_{tf} is the flange width of bearing stiffener, which is taken as 75 mm. In this parametric study, the depth of bearing stiffener is taken 25 mm less than the clear distance between the flanges. The variation of service and failure loads of beams having different geometric configurations and length of beams, w.r.t. the size of bearing plate is shown in Fig. 6.16. It is interesting to observe that the beams having length of bearing plate lesser than the flange width of T-shaped bearing stiffener failed due to failure of bearing stiffener, while in the other beams failure criterion is satisfied below the web-flange junction as observed in previous section. It is worth mentioning that the service load of beams increases with increase in the length of bearing plate, while the failure load depends on the mode of failure such as local buckling and crushing of stiffener which lead to the pre-mature failure of the beams as shown in Figs. 6.16 (a), (b) and (c). Beams having h_w/t ratio equal to 40 and length of bearing plate equal to $1.4b_t$ and $2.1b_t$ are failed due to buckling (see Fig. 6.17), therefore failure load is lesser than beam with bearing plate of length $2.8b_t$. The failure of beams having L/d ratio 3 with bearing plates of sizes $0.7b_t$, $1.4b_t$ and $2.1b_t$ and beam having L/d ratio 7 with length of bearing plate $0.7b_t$ is due to the failure of bearing stiffener. It is due to the lesser length of bearing plate than flange width of bearing stiffener. In other beams stresses exceed the strength of the beam below the compression web-flange junction. In case of beams having L/d ratio 11 and a/b_{tf} greater than 1.5, local buckling of web occurred, therefore failure load of the beams having $a/b_{tf} \leq 1.5$ have slightly higher failure load.

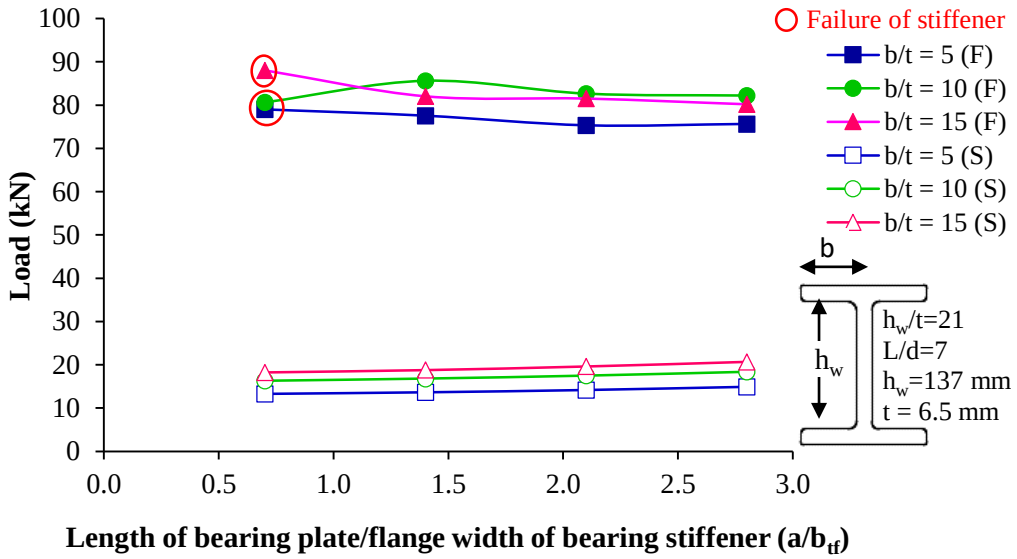

(a) width-to-thickness ratios (b/t)

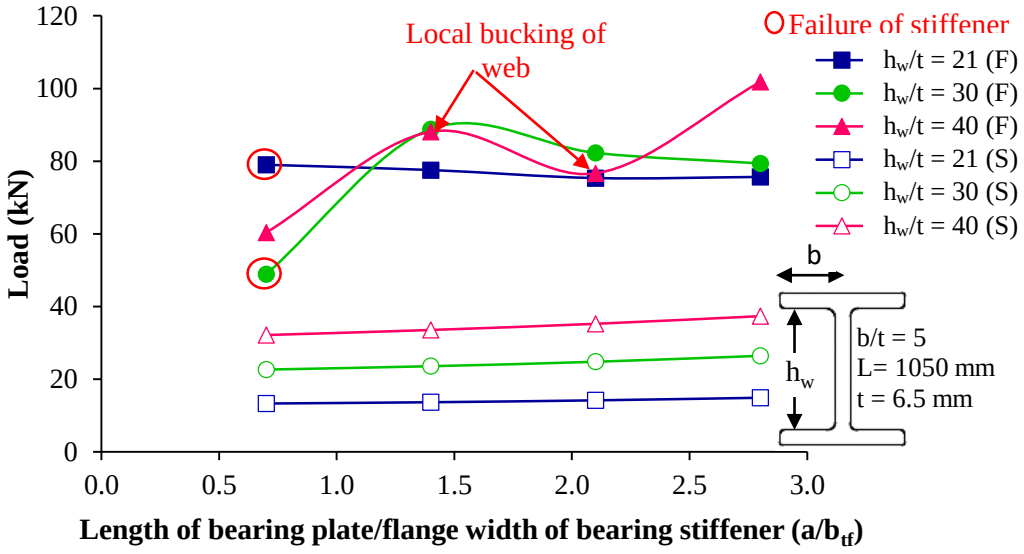

(b) depth-to-thickness ratios (h_w/t)

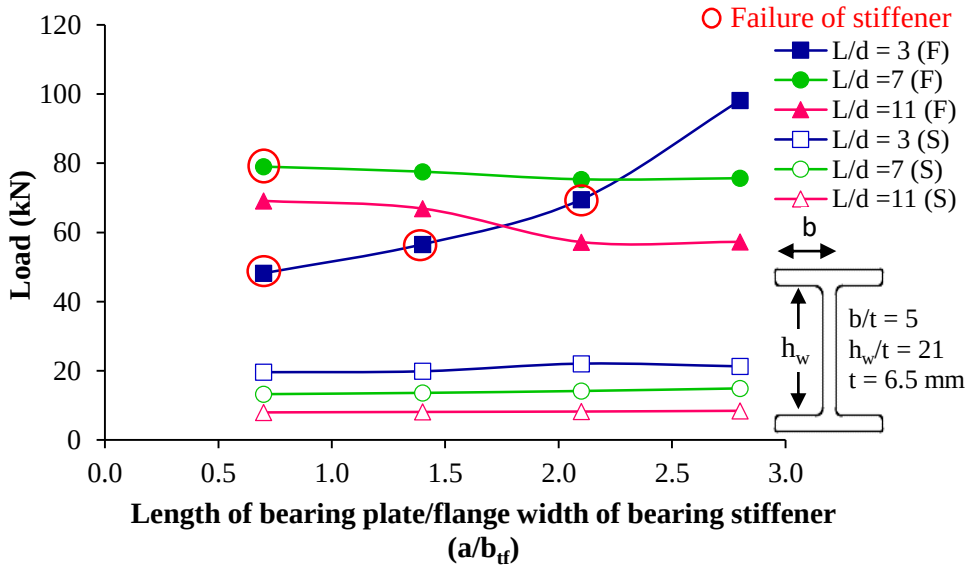

(c) length-to-depth ratios (L/d)

Fig. 6.16. Influence of length of bearing plate/flange width of bearing stiffener on failure and service loads of beams.

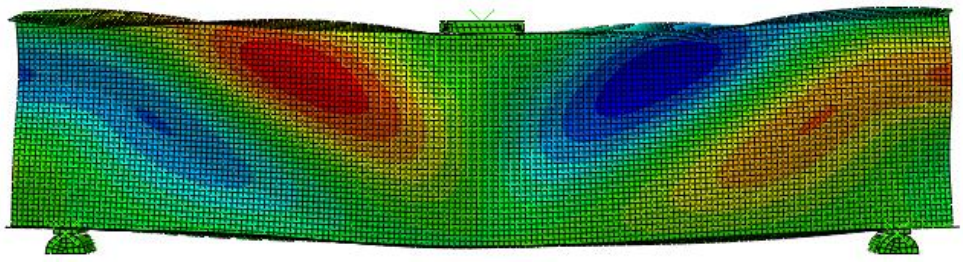

Fig. 6.17. Local buckling of beam having bearing plate of size $0.7b_{tf}$ and h_w/t ratio 40.

6.4.4 Influence of length of cover angle

In this study, the length of cover angle (L_{ca}) is taken as L/2, L/4 and L/6, where L is the length of the beam. Cover angle is provided at compression web-flange junction under the bearing plate and length of bearing plate is 0.15L. The width of connected leg of cover angle under flange is 34.25 mm and width of other connected leg over web is 50 mm. The service and failure loads of the beams having different cross-section and lengths provided with bearing plate of different lengths are presented in Fig. 6.18(a). From Fig. 6.18(a), it is observed that failure load of beams initially increases with increase in length of cover angle (i.e., L/6 to L/4), and later it becomes almost constant, while the service load remains constant with different length of cover angle. In another study of beams having same length but different depths, initially failure load increases with increase in length of cover angle from L/6 to L/4 but later it becomes constant with further increase in the length of cover angle. As expected, service load of beam having h_w/t ratio 40 is more than that of beams having h_w/t ratios 21 and 30, because the depth of beams (h_w/t ratio 40) is higher than other beams. While the failure load of beams having h_w/t ratio 40 and cover angle of lengths L/4 and L/2 is lesser than that of beams having h_w/t ratios 21 and 30, due to the buckling (see Fig. 6.18(b)) which leads to the premature failure of beams. Fig. 6.18(c) shows that failure load of beams having L/d ratio 3 and cover angle of length L/6 and L/4 is lesser than beams having L/d ratios 7 and 11, and having same length of cover angle. It is because the length of cover angle is lesser than the width of bearing plate, hence failure criterion is satisfied at web under the bearing plate and cover angle is ineffective to enhance the failure load of beams. From these observations, it is concluded that length of cover angle should be more than the length of bearing plate and increase in the service load is not significant in comparison with the increase in failure load of beam when length of cover angle is increased from L/6 to L/4.

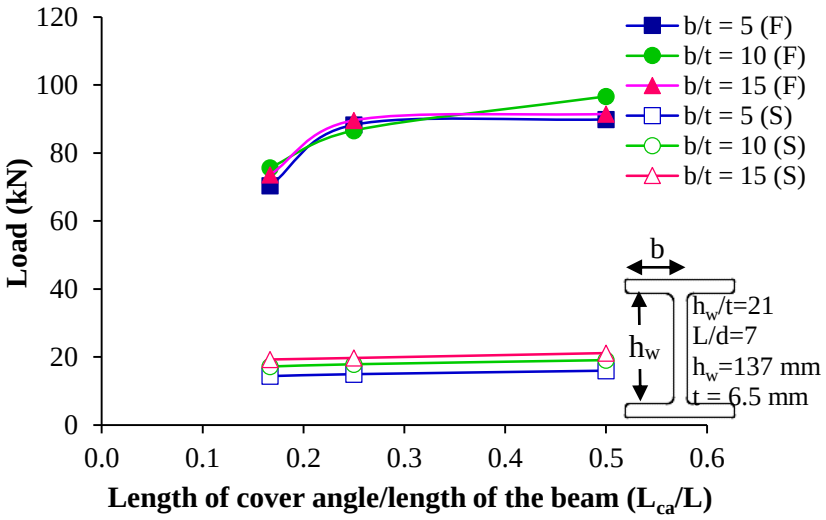

(a) different width-to-thickness ratios (b/t)

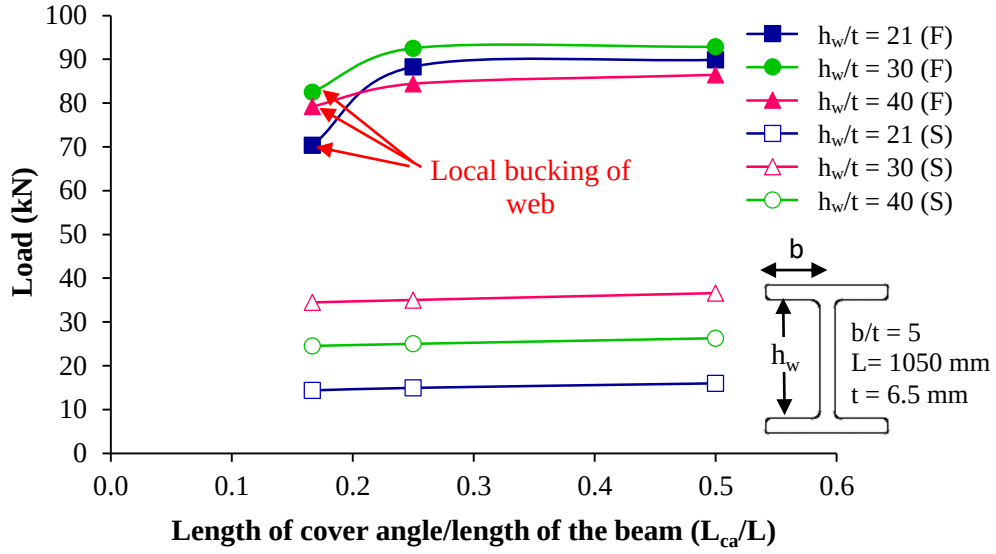

(b) different depth-to-thickness ratios (h_w/t)

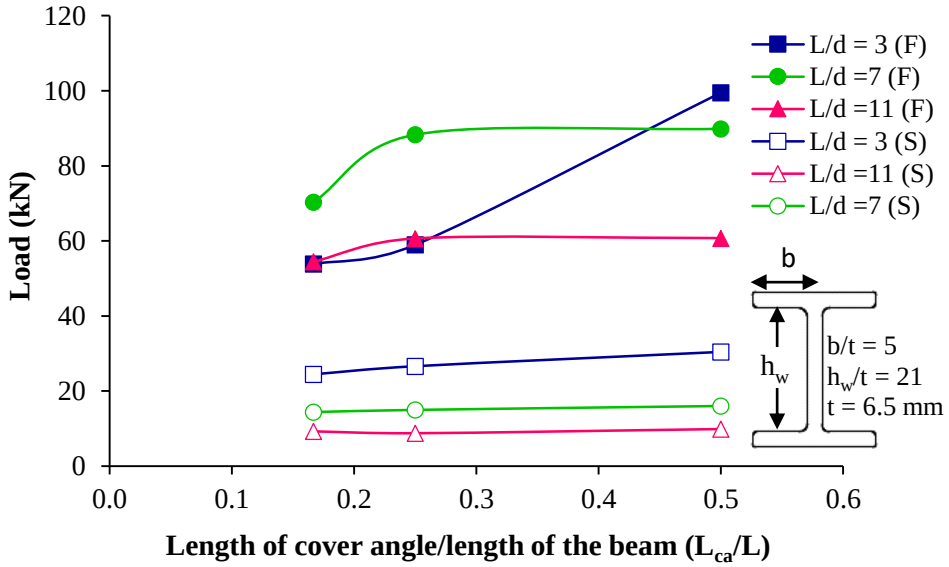

(c) different length-to-depth ratios (L/d)

Fig. 6.18. Influence of length of cover angle on failure and service loads of beams.

6.4.5 Influence of length of carbon fiber layers

In this section, two layers of carbon fibers (0/90) are attached on each side of compression web-flange junction of beam under the load bearing plate and behave like a carbon fiber cover angle. The length of leg of carbon fiber angle at flange is 34.25 mm and at web is 50 mm, while the length of carbon fiber angle (L_{cl}) on different beams is L/6, L/4 and L/2, where 'L' is the length of the beam. Mechanical properties of carbon fiber layers are given in Table 3.9 (Chapter 3). The failure and service loads of beams with different

length of carbon fiber layer and different b/t ratios are shown in Figs. 6.19(a), 6.19(b) and 6.19(c). From Fig. 6.19(a), it is observed that service load of the beam increases with increase in the length of carbon fiber angle and the failure load initially increases and later it becomes constant. The failure of beams with carbon fiber layer of length L/6 (i.e., $L_{cl}/L = 0.167$) is due to the local buckling of flanges as shown in Fig. 6.20(a), while in beams having carbon fiber of lengths L/4 and L/2, failure criterion satisfies before local buckling of flanges. It is stated that the carbon fiber of length equals to or greater than L/4 is effective in enhancing the buckling load of beams. Beams with carbon fiber layers of lengths L/4 and L/2, have almost equal failure load, because of the delamination failure of web under the carbon fiber layers. In case of beams having h_w/t ratios 21 to 40 and same L/d ratio, failure is due to local buckling of web, because of diagonal stresses produced from corners of carbon fiber angle as shown in Fig. 6.20. Although the height of beams having h_w/t ratio 40 is higher than that of h_w/t ratio 30, but the failure load is less. It is because with increase in h_w/t ratio, chances of local buckling of web increases. It is also observed that the failure load of beams with carbon fiber angle is lesser than the beams with cover angle having different h_w/t ratios. Failure load of beams having L/d ratio 3 and carbon fiber angle of lengths L/6 and L/4, is predicted based on the failure criterion satisfied under the bearing plate, as observed earlier in case of beams with cover angle.

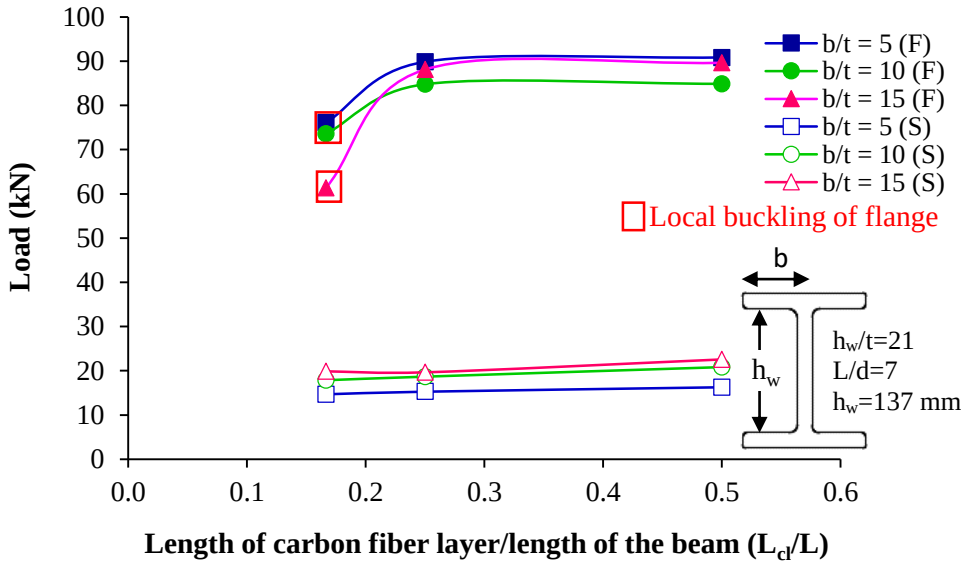

(a) width-to-thickness ratios (b/t)

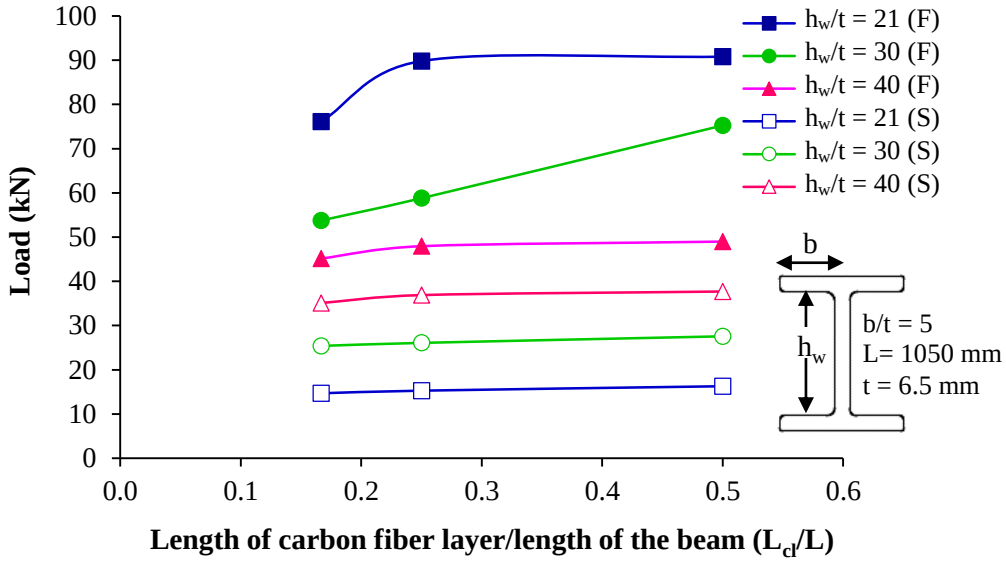

(b) depth-to-thickness ratios (h_w/t)

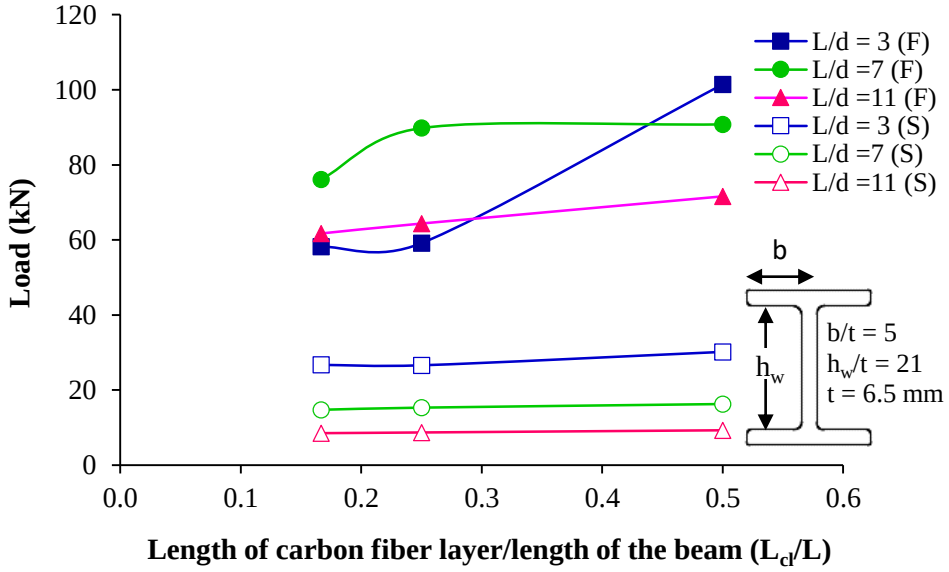

(c) length-to-depth ratios (L/d)

Fig. 6.19. Variation of service and failure loads of beams w.r.t. ratio of length of carbon fiber layer/length of the beams.

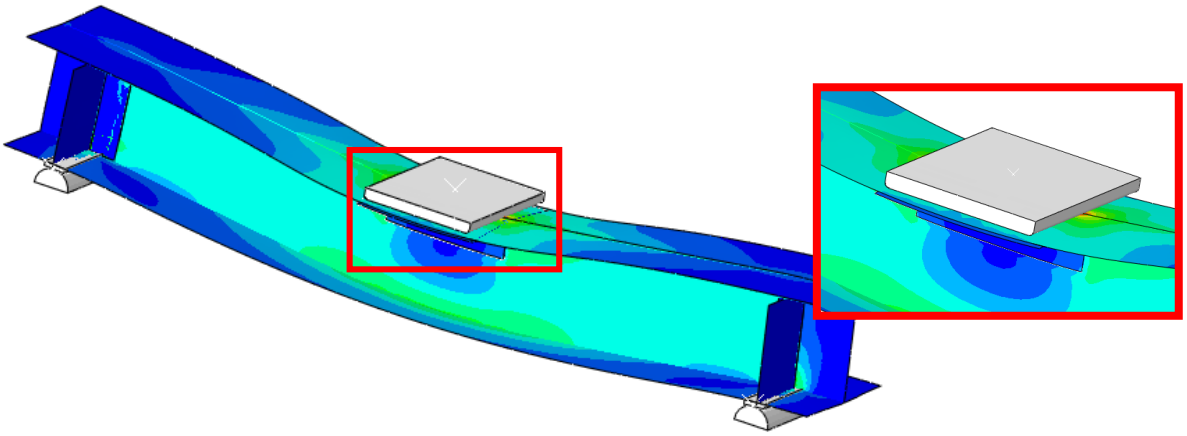

(a) b/t ratio 10 and carbon fiber layer of length L/6

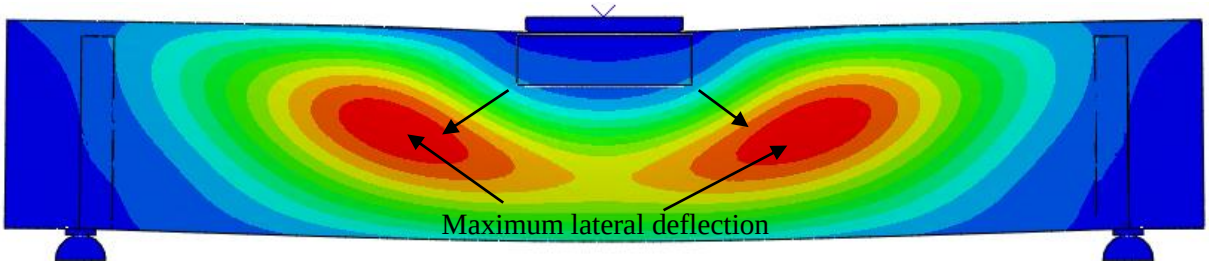

(b) $h_w/t = 30$

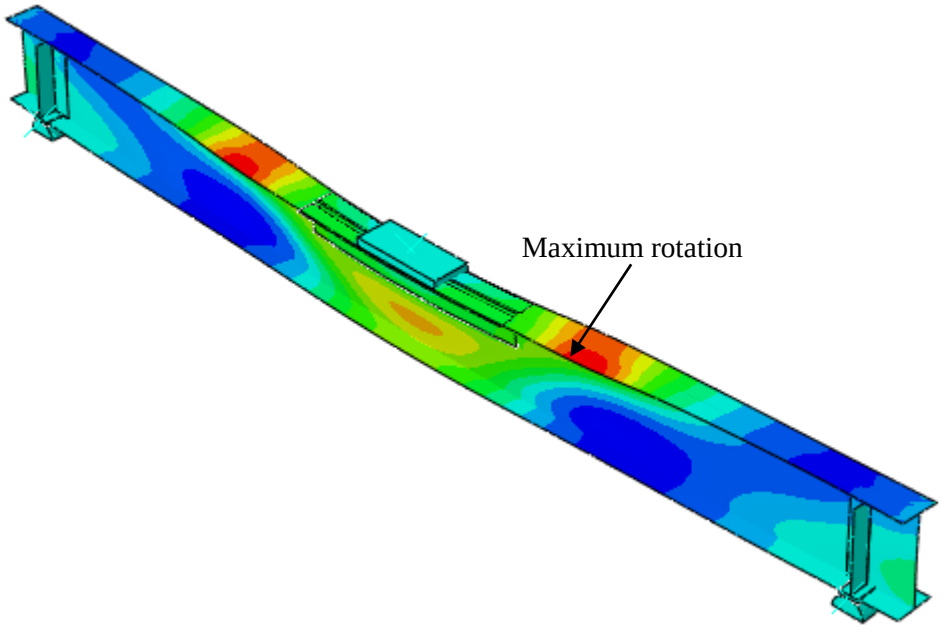

(c) L/d = 11 and carbon fiber angle of length L/4.

Fig. 6.20. Local buckling of beams having carbon fiber layer.

6.4.6 Influence of length of cover plate

In this section, the influence of cover plate length on the service and failure loads of the beam is investigated. The width of cover plate provided is equivalent to the width of compression flange, i.e., 65 mm and the length (L_{cp}) is varied from L/6 to L/2. The variation of loads w.r.t. length of cover plate and b/t ratio is shown in Fig. 6.21(a), while for beams with different h_w/t and L/d ratios is shown in Figs. 6.21(b) and 6.21(c), respectively. From Fig. 6.21(a), it is observed that length of cover plate hardly effects the failure load of beams, while the small increase in the service load with increase in cover plate length is noted. The failure criterion is satisfied under load bearing plate at web as observed in the study of beams without any stiffening element, i.e., beams with bearing plate only. However, the failure load is little higher than beam having bearing plate only. Fig. 6.21(b) shows that length of cover plate has significant effect on the failure load of the beam having h_w/t ratio 40. It means that for slender webs, cover plate may be beneficial in enhancing the load capacity. From Fig. 6.21(c), it is noted that in comparison to other beams, length of cover plate has significant effect on failure load of the beams having L/d ratio 11. The failure load of beams of L/d ratio 3 and with lengths of cover plate L/6 and L/4, is higher than that of beam without stiffening element, (i.e., beam having bearing plate only) and it is equivalent to that of beam with cover angle and/or carbon fiber angle.

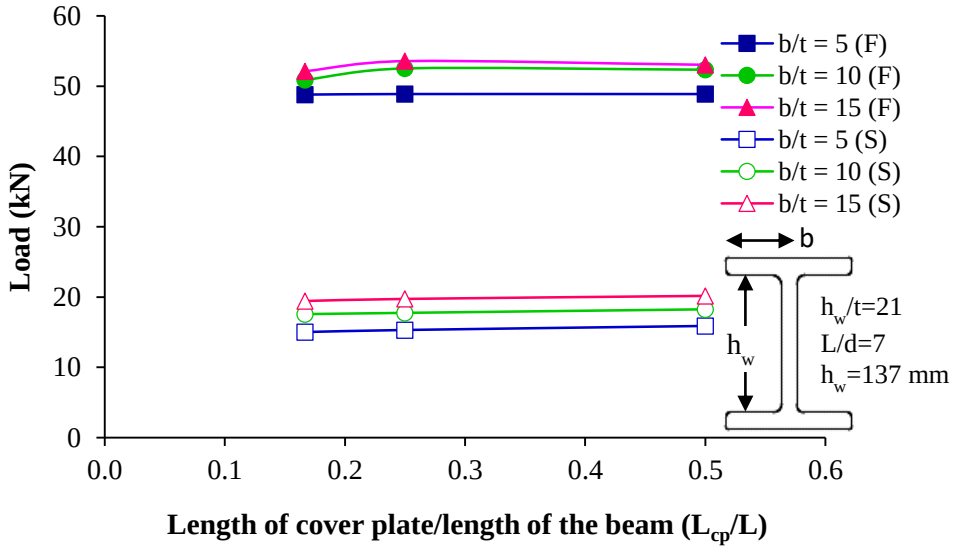

(a) different b/t ratios

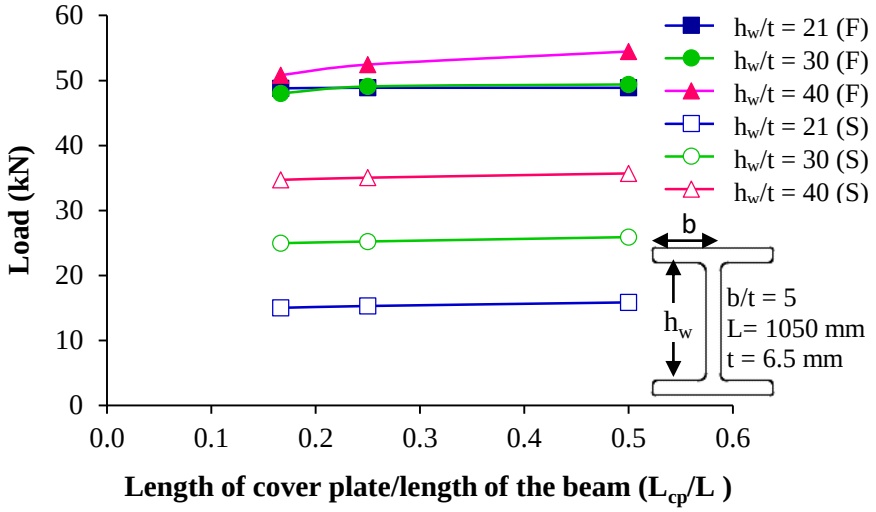

(b) different h_w/t ratios

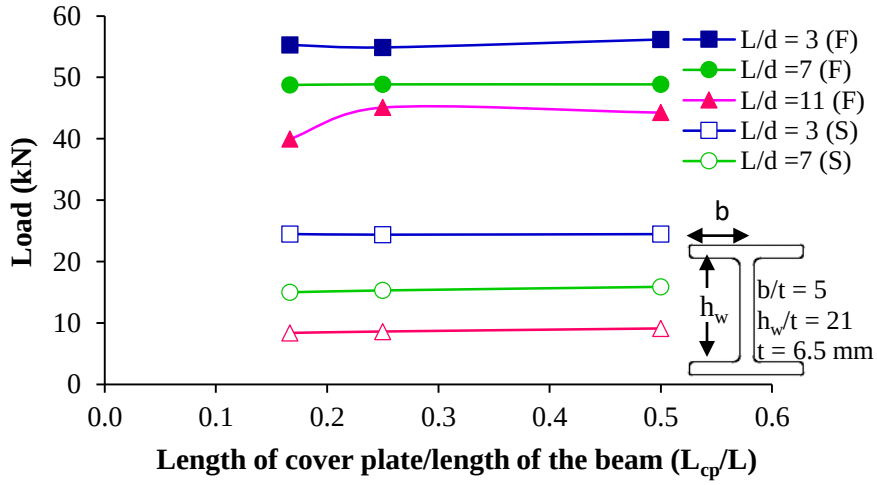

(c) L/d ratios of beams

Fig. 6.21. Variation of service and failure loads of beams.

6.4.7 Influence of spacing of bolts and sizes of web plate

In this section, failure load is determined for horizontal and vertical edge distances of bolts from the edges of the web plate. Further, the effect of width and height of web plate on the failure and service loads of the beams is investigated for beams having b/t ratio 5, h_w/t ratio 21and L/d ratio 7. Bearing plate produces high bearing stresses on the web of I-section and web plate, as well as bending stresses is maximum at the mid span. Hence, it is important to study the effect of vertical distances of holes from bearing plates and horizontal distances of bolts from the mid-span of the beams. Therefore, failure load of the beam is determined for vertical edge distances (center of the hole to edge of the plate) of 20, 25, 30 and 35 mm, and the same edge distance is provided for the bottom row of bolts. The horizontal edge distance of the bolts

was kept same, i.e., 20 mm. The failure loads obtained from failure criterion are given in Table 6.4. It is observed that failure load is less at vertical edge distance of 20 mm than that for 25 mm, because the edge distance 20 mm is closer to the bearing plate (see Fig. 6.22). Moreover, failure load is constant with further increase in the vertical edge distance, i.e., distance of bolts from web-flange junction. It is because the distance of the bolts from the web-flange junction is very short, i.e., holes are nearer to the web-flange junction. Hence, the failure load of the beams is less in comparison with other web-flange distance.

In case of beams having different horizontal edge distances and constant vertical edge distance (25 mm), failure load decreases as edge distance increases, because the horizontal distance of bolts from the mid-span decreases (i.e., holes are more closer to the section having maximum bending moment). Using these observations, further study is conducted on horizontal and vertical edge distances of 15 mm and 25 mm, respectively. The failure and service loads of beams having different length and depth of web plate is presented in Table 6.4. It is interesting to note that failure load decreases and service load increases with increase in the length of the web plate. As the length of web plate increases, holes come closer to the line of diagonal bearing stresses at 45^{o} produced from the edge of bearing plate, which lead to the failure near to the holes. It is worth noting that with increase in the depth of the web plate, failure load decreases. This is due to the increase in the tensile stresses with increase in the distance from the neutral axis (towards the bottom flange), as a result of this, high tensile stresses occur at the holes of the bolted connection.

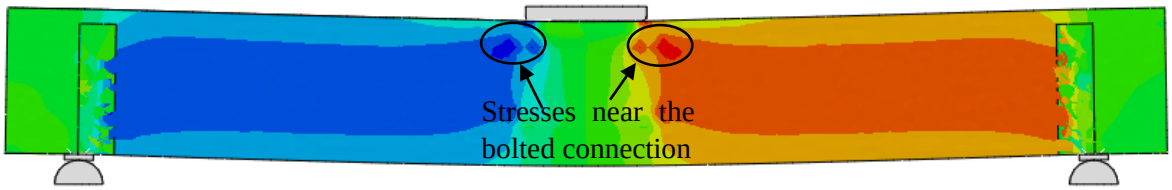

Fig. 6.22. Variation of stresses near the bolted connection.

Table 6.4 Failure and service loads of beams stiffened with web plate having different edge distances and sizes of plate.

Vertical distance		**Horizontal distance**		**Length of web plate**			**Depth of web plate**		
Edge distance♣ (mm)	**Failure load (kN)**	**Edge distance♦ (mm)**	**Failure load (kN)**	**b_w/L♠**	**Failure load (kN)**	**Service load (kN)**	**d_w/D♥**	**Failure load (kN)**	**Service load (kN)**
20	70.48	15	78.04	0.19	84.56	15.48	0.70	83.93	15.37
25	73.79	20	70.48	0.22	83.10	15.65	0.63	70.17	15.37
30	73.99	25	69.22	0.24	80.54	15.96	0.56	71.69	15.36
35	74.01	30	70.53	0.26	74.34	16.2	0.50	84.21	15.26

♣Horizontal edge distance 20 mm and size of plate 200 x 115 mm (width x height)
♦Vertical edge distance 25 mm and size of plate 200 x 115 mm (width x height)
♠Height (d_w) of the plate is 115 mm, horizontal and vertical edge distances of 15 mm and 25 mm, respectively.
♥Width (b_w) of the plate is 200 mm, horizontal and vertical edge distances of 15 mm and 25 mm, respectively.

6.5 Flexural behavior of castellated beams

This section demonstrates the numerical modelling of FRP castellated beams with different sizes and shapes of openings. The experimental investigation on FRP beams with different angles of edge of opening is explained in Chapter 4 (Section 4.8). The validation of the numerical model with experimental results and further parametric study conducted on FRP castellated beams is explained in the following sections.

6.5.1 Validation of numerical models

From the experimental investigation, it was seen that the beam failed due to the tearing and delamination of layers near the corner of the openings. Similarly, high stress is also observed in the ABAQUS model around the corners of the openings (see Fig. 6.23) and the failure criterion (Eq. 6.1) also satisfied at this location. The failure of the web-flange junction was not seen in castellated beams. The comparison of load-vs-deflection responses obtained from experimental and numerical models is shown in Fig. 6.24. In Figs. 6.24(a) and 6.24(b), specimen ID with last letters 'E' and 'AB', denotes the experimental and ABAQUS responses, respectively. It is observed that flexural responses and failure loads obtained from experimental and numerical models show the good agreement. Failure load obtained from the failure criterion (Eq. 6.1) is approximately equal to the experimental failure load of the beam.

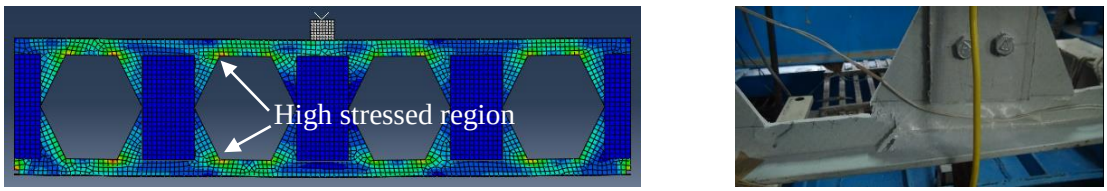

(a) Stresses in beam under loading (b) Cracking of beam (Experimental)

Fig. 6.23. Flexural deformation of castellated beam under three-point loading.

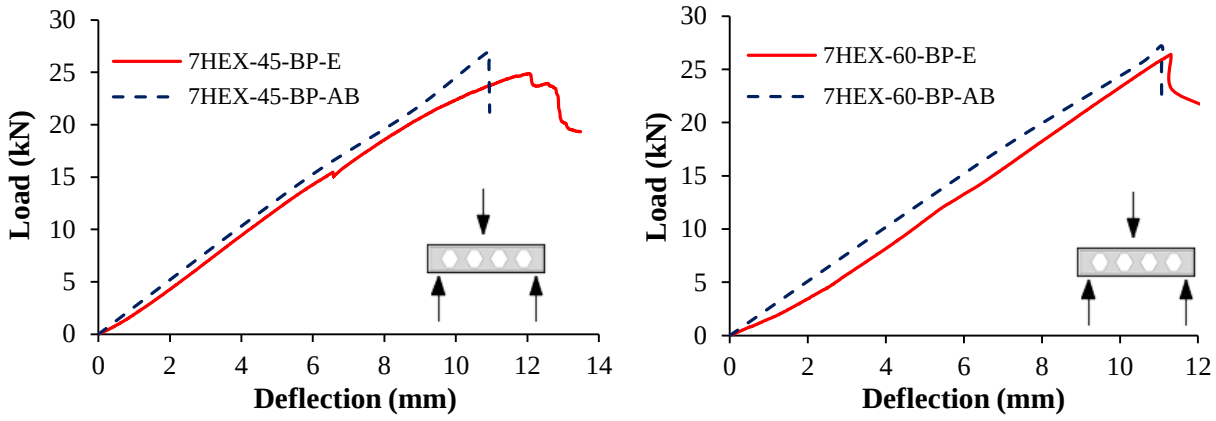

(a) Cutout angle 45º (b) Cutout angle 60º

Fig. 6.24. Comparison of experimental and numerical flexural response of beams having hexagonal cutout.

6.5.2 Parametric study of castellated beams

This section demonstrates the effect of different depths of the opening and shapes of cutout on the failure and service loads of the castellated beams. In this study, ratio of depth of beam-to-depth of opening (D/D_o) is varied from 1.25 to 1.75, with constant depth of beam (D), center-to-center spacing (S) of cutouts and number of cutouts in the beam. This effect is observed for beams having hexagonal and circular openings in the beams. The beams having hexagonal openings, edge of cutout makes 45º and 60º angle with longitudinal axis and the fillet radius at each corner of opening is 5 mm. Moreover, the effect of fillet radius of 20 mm at corner of the hexagonal opening of angle 60º is also investigated and those beams are called as sinusoidal openings. The area of sinusoidal openings is equal to the area of hexagonal openings. The service load is determined at the limit state of deflection, i.e., L/300 (L is the span length).

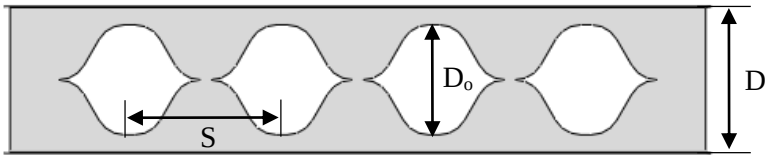

Fig. 6.25. Castellated beam with hexagonal opening.

6.5.3 Results and discussion

Under the flexural loading, maximum stresses produced near the edge of the opening as depicted in Fig. 6.26, and the failure criterion is also satisfied at this location. The comparison of failure and service loads of the castellated beams with different sizes of opening is presented in Table 6.5. In Table 6.5, the beam having circular and sinusoidal openings is represented by 'Circular' and 'Sine fillet', respectively, while

the beam having hexagonal opening edge angle 45° and 60° is denoted by 'HEX-45' and 'HEX-60', respectively. It is noted that with decrease in the S/D_o ratio (due to increase in the depth of opening, D_o) the size of the opening increases, and failure load of the beam decreases. It is because of the effective area of T-section to resist shear and bending stress decreases. The same effect is observed in each shape of cutout. It is worth noting that even though the area of opening of both 45° and 60° angle of hexagonal cutout is same, but failure load of the 60° angle cutout is higher than that for the 45° angle, while the service load of the 45° angle hexagonal cutout is higher. Higher failure load is attributed to the higher shear area present in the T-section. In case of beams having sinusoidal opening, the failure load is higher than that for beam having hexagonal cutouts and is equivalent to beam having circular opening. In sinusoidal opening, stress concentration near the edge of the openings is lesser than beams having hexagonal opening, hence it has higher failure load. Beams having circular cutout have higher area of cutouts than other shapes of cutout, so it exhibits lower stiffness and service loads than other beams. Stress concentration is reduced highly for beams with circular cutouts. Therefore, beam with circular openings show high failure load than that of other castellated beams.

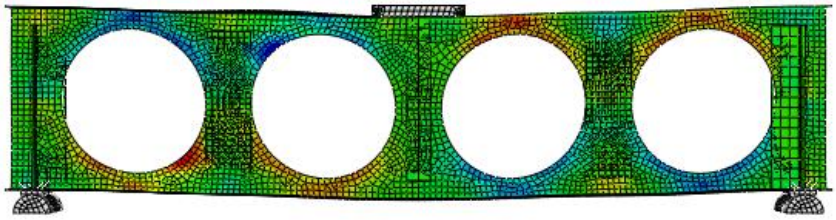

(a) Circular openings

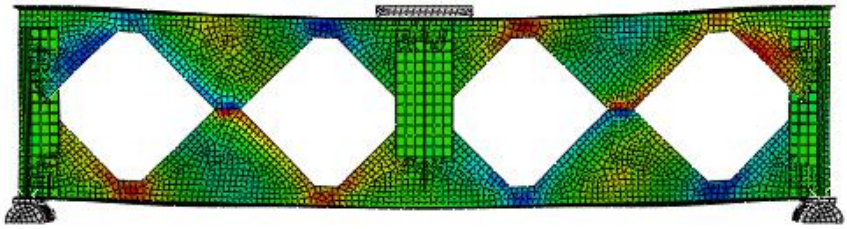

(b) Hexagonal openings, angle of opening edge is 45° w.r.t to longitudinal axis of beam (HEX-45)

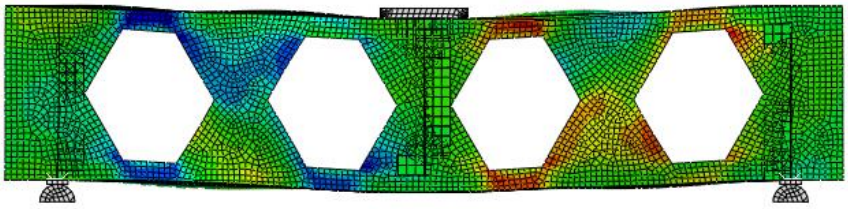

(c) Hexagonal openings, angle of opening edge is 60° w.r.t to longitudinal axis of beam (HEX-60)

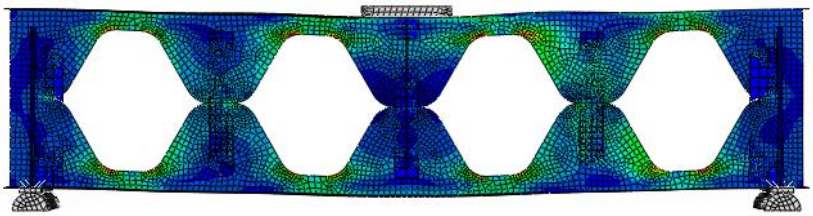

(d) Sinusoidal openings

Fig. 6.26. Stress variation in beams having different shapes of openings.

Table 6.5 Service and failure loads of the castellated beams with different sizes of openings.

Shape of cutout	**S/D_o ***	**D/D_o ♣**	**Area of cutout (m^2)**	**Service load (kN)**	**Ultimate load (kN)**
Circular	1.46	1.33	0.025	7.25	31.24
Circular	1.38	1.29	0.028	7.54	32.27
Circular	1.31	1.25	0.031	7.83	33.19
HEX-60	1.46	1.33	0.024	8.91	27.23
HEX-60	1.38	1.29	0.025	9.51	29.13
HEX-60	1.31	1.25	0.026	10.11	31.03
HEX-45	1.46	1.33	0.024	9.03	26.95
HEX-45	1.38	1.29	0.025	9.66	27.35
HEX-45	1.31	1.25	0.026	10.29	27.76
Sine fillet	1.46	1.33	0.025	8.45	28.64
Sine fillet	1.38	1.29	0.028	8.94	30.16
Sine fillet	1.31	1.25	0.031	9.43	31.68

* 'S' Center-to-center spacing between the openings
♣ 'D_o' is depth of the opening
♣ 'D' is the total depth of the castellated beam

6.6 Conclusions

This chapter presents the numerical modeling of stiffened and unstiffened FRP I-beams, and FRP castellated I-beams. The flexural response of FRP I-beams obtained from numerical models is compared with experimental and analytical results. After validation of numerical modelling, a parametric study is conducted to assess the potential role of stiffening elements in enhancing the strength of beam. The parametric studies include the effect of length of bearing plate, material properties, and sizes of stiffeners

on different flange width-to-thickness ratios, depth-to-thickness ratios and length-to-depth ratios of the beam. Moreover, the effect of different shapes and sizes of openings on the flexural response of the castellated I-beams is investigated. From this study, following concluding remarks have been made

1. Formulae available in codes give significantly higher or lower failure load than that obtained from experimental investigation. Delamination failure criterion gives the failure load closer to experimental tests.
2. The use of stiffening elements proves to be effective in many aspects such as increasing the stability, failure and service loads of beams.
3. Service load increases with increase in the length of bearing plate. While the failure load of beams increases up to certain length of bearing plate, later it becomes constant. This effect is observed in beams having different width-to-thickness ratios, effective depth-to-thickness ratios, and length-to-depth ratios.
4. Failure load of beams increases with increase in longitudinal-to-transverse Young's modulus ratio (E_1/E_2) of the beams, while it decreases with increase in the longitudinal Young's modulus-to-shear modulus ratio (E_1/G_{12}). Moreover, the service load decreases with increase in E_1/E_2 and E_1/G_{12} ratio of the beams.
5. Under flexural loading, bearing stiffeners of a beam fail, if the length of bearing plate is less than the flange width of T-shaped bearing stiffener. Similarly, if length of cover angle or carbon fiber angle is less than the length of bearing plate, then the failure load is equivalent to the beams having bearing plate only.
6. With increase in the area of openings of castellated beams, the failure and service load decreases, while the depth of the beam increases.